Review

Planar Printed Structures Based on Matryoshka Geometries: A Review

Alfredo Gomes Neto , Jefferson Costa e Silva , Joabson Nogueira de Carvalho , Custódio Peixeiro *

Posted Date: 19 February 2024

doi: 10.20944/preprints202402.1017.v1

Keywords: printed circuits; microstrip; ring resonators; Matryoshka sets; frequency selective surfaces; filters; antennas; sensors

Review

Planar Printed Structures Based on Matryoshka Geometries: A Review

Alfredo Gomes Neto [1], Jefferson Costa e Silva [1], Joabson Nogueira de Carvalho [1] and Custódio Peixeiro [2,*]

[1] Group of Telecommunications and Applied Electromagnetism (GTEMA), Instituto Federal da Paraíba, João Pessoa, Brazil
[2] Instituto de Telecomunicações, Instituto Superior Técnico, University of Lisbon, Portugal
* Correspondence: custodio.peixeiro@lx.it.pt

Abstract: A review on planar printed structures that are based on Matryoshka-like geometries is presented. These structures use the well-known principle of Matryoshka dolls that are successively nested inside each other. The well-known advantages of the planar printed technology and of the meandered nested Matryoshka geometries are combined to generate miniaturized, multi-resonance and/or wideband configurations. Both metal and complementary slot structures are considered. Closed and open configurations are analyzed. The working principles are explored do get physical insight of their behavior. Low cost and single layer applications as frequency selective surfaces, filters, antennas, and sensors, in the microwave frequency region, are reviewed. Potential future research perspectives and new applications are discussed.

Keywords: printed circuits; microstrip; ring resonators; Matryoshka sets; frequency selective surfaces; filters; antennas; sensors

1. Introduction

The name Matryoshka comes from the well-known Russian dolls, shown in Figure 1, that are successively nested inside each other. It has been used to refer to nested sets in many areas of electrical and electronics engineering, such as: electronics packaging [1], implantable medical devices [2], biomedical imaging [3], computer network security [4], silicon compounds [5], software protection [6], internet-of-things [7], image retrieval [8] and reconstruction [9], cancer gene analysis [10], cellular biophysics [11], cloud computing [12], 5G network slicing [13], acoustic wave resonators [14], pattern recognition [15] and astronomy [16]. It has also been used associated with planar printed configurations. This combination of printed circuits with Matryoshka-like geometries benefits from the well-known advantages of printed planar technology (low profile, lightweight, compactness, low cost, easy fabrication and integration of electronic components, wide range of characteristic impedances) and the multiband (or wideband) behavior and miniaturization associated with Matryoshka configurations. The Matryoshka-like scheme was used for the first time, in planar printed circuit structures at the Group of Telecommunications and Applied Electromagnetism (GTEMA) from the Instituto Federal da Paraíba, in João Pessoa, Brazil. A multi-resonant frequency selective surface (FSS) was proposed in 2014 [17,18]. Since then, the work in these planar printed structures based on Matryoshka geometries has progressed steadily at GTEMA as reported in many MSc thesis [17,19-31] and associated publications [32-46]. Different applications have been envisaged, such as, FSSs [17-19,21,23,24,27,32,33,36,38-40,42], filters [20,22,26,30,37,43,46], antennas [25,28] and sensors [29,31,34,35,41,44,45]. All these applications are motivated mainly by the huge importance of new telecommunication systems, particularly mobile communication networks, with emphasis in the recently deployed 5G systems and the closed associated Internet-of-Things (IoT). New ideas and perspectives are being explored to further develop these new types of structures. However, having worked on it for about then years the topic is already sufficiently mature to justify the publication of

 doi:10.20944/preprints202402.1017.v1

a review paper. Therefore, the goal of this paper is precisely to present a review on the work done in the field of planar printed structures based on Matryoshka geometries. The paper is organized in seven sections. After this introductory section, section 2 deals with the printed planar Matryoshka geometry. The Matryoshka cell is described, and the corresponding working principles are analyzed. Sections 3, 4, 5 and 6 are dedicated to the description of the use of this type of cell in FSSs, filters, antennas, and sensors, already reported applications, respectively. At the end, section 7 contains the main conclusions and the perspectives of present and future developments.

Figure 1. Example of a Russian Matryoshka with 9 nested dolls.

2. The Matryoshka Geometry

The Matryoshka geometry is based on concentric rings. As shown in Figure 2, Matryoshka geometries have been conceived as an evolution of the split ring resonators (SRRs). Starting with a set of rings (so far homothetic), introduce a gap in each one and then connect the consecutive rings near the gaps. However, differently from the SRR [47], the rings are connected. As in an SRR, the rings may take different shapes, from simple ones (as square or circular) to other, more complex, canonical, or non-canonical geometries. Matryoshka geometries have been implemented in printed circuit board (PCB) technology, both with and without ground plane. As the SRR, they can be formed by metal strips or by slots in the metal (complimentary configurations). As complimentary configurations Matryoshka geometries have been used in defected ground structures (DGSs) [30,48] and FSSs [24].

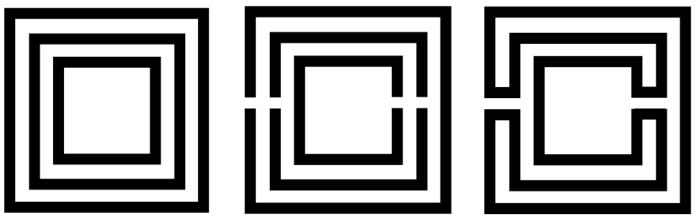

Figure 2. Example of evolution from concentric rings to a Matryoshka geometry. a) Concentric rings without gaps. b) SRR. c) Matryoshka geometry.

For a specific type of Matryoshka geometry there are two sub-types: the open and the closed. It is open when there is a gap in the smaller inner ring (Figure 3). As it will be detailed in the next sections, this gap has a remarkable effect on the structure's characteristics, namely on its resonance frequencies. Due to the metal continuity, in the closed configuration, for the first resonance

$$L_{ef} \approx \lambda_{refclose}, \quad (1)$$

whereas for the open one

$$L_{ef} \approx \lambda_{refopen}/2, \quad (2)$$

where L_{ef} is the effective length of the structure and λ_{ref} the effective wavelength [19] for the first resonance. Naturally, there are other (higher order) resonances. This difference in the behavior of the closed and the open structure can be explained by the continuity required by the closed structure and the interference standing wave pattern imposed by the reflection at the gap of the open structure's inner ring. This means that, for structures with the same dimensions, the open structure has a first

Preprints.org (www.preprints.org) | NOT PEER-REVIEWED | Posted: 19 February 2024 doi:10.20944/preprints202402.1017.v1

resonance frequency that is approximately half the one of the closed structure. In other words, for the same first resonance frequency, the open structure has an equivalent electrical length that is approximately half of the one of the closed structure, meaning a much more effective miniaturization capability.

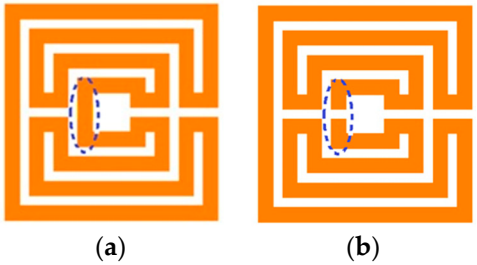

(**a**) (**b**)

Figure 3. Example of Matryoshka geometries. a) Closed. b) Open.

The Matryoshka configurations are highly meandered, and the total area occupied is defined by the external ring. The physical parameters of an open square Matryoshka configuration, with four rings, are indicated in Figure 4. For the closed Matryoshka geometry there is no gap at the inner ring (s=0). When a Matryoshka geometry is used in an FSS it is also necessary to specify the unit-cell size.

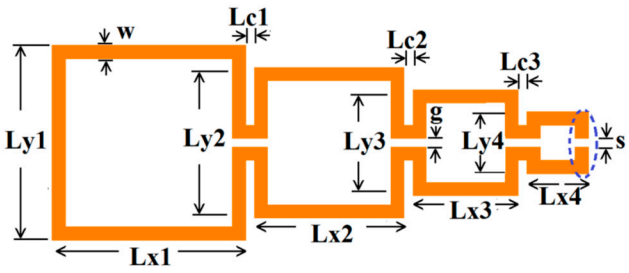

Figure 4. Open Matryoshka geometry, expanded, with the definition of its physical parameters.

The average perimeter of the closed geometry (P_N), corresponds to the physical length defined at the middle of each segment, can be obtained using equation 3. For the open geometry s must be subtracted from P_N.

$$P_N = 2\left[\sum_{n=1}^{N}\left(L_{xn} + L_{yn}\right) + \sum_{n=1}^{N-1} L_{cn} - 2Nw - (N-1)g\right] \quad (3)$$

In printed planar structures it is also necessary to specify the substrate characteristics (ε_r - relative electric permittivity, h – thickness, and tanδ – loss tangent) and the presence or absence of the ground plane. In both cases the structures are transversally non-homogeneous, and an equivalent homogenous medium can be conceived. For the commonly used substrates, with normal magnetic behavior, an effective relative electric permittivity (ε_{ref}), and an effective wavelength (λ_{ef}) can be defined.

$$\lambda_{ef} = \frac{\lambda_0}{\sqrt{\varepsilon_{ref}}} \quad (4)$$

where λ_0 is the wavelength in vacuum. The procedure used to calculate ε_{ref} depends on the type of configuration used which is associated with the envisaged application. For filters a microstrip structure has been used, whereas for FSSs a simple substrate without ground plane has been selected. For antenna applications, so far, only microstrip structures with DGSs have been employed.

There are some features of the Matryoshka geometries that depend on the specific type of structure and application. These specific features will be detailed in the next sections, where applications as FSSs, filters, antennas and sensors are analyzed. However, there are some features

 doi:10.20944/preprints202402.1017.v1

that are intrinsic of the Matryoshka geometries and therefore are common to all type of applications. These common features will be analyzed here using microstrip filters as application examples.

There are different formulas to obtain the ε_{ref} of a microstrip line, a simple non-dispersive model, valid for low frequency, is given in equations 5 to 7 [49].

$$\varepsilon_{ref} = \frac{\varepsilon_r + 1}{2} + \frac{\varepsilon_r - 1}{2}\left(1 + 10\frac{h}{w}\right)^{-ab} \tag{5}$$

$$a = 1 + \frac{1}{49} ln\left[\frac{\left(\frac{w}{h}\right)^4 + \left(\frac{w}{52h}\right)^2}{\left(\frac{w}{h}\right)^4 + 0.432}\right] + \frac{1}{18.7} ln\left[1 + \left(\frac{w}{18.1h}\right)^3\right] \tag{6}$$

$$b = 0.564\left(\frac{\varepsilon_r - 0.9}{\varepsilon_r + 3}\right)^{0.053} \tag{7}$$

For a 2.0 mm wide microstrip line printed on a FR4 substrate with ε_r=4.4 and h=1.5 mm equation 5 leads to ε_{ref}=3.23.

The outline of a microstrip filter, with an open Matryoshka geometry of two rings, is shown in Figure 5. The input and output microstrip lines are 2.8 mm wide (50 Ohm characteristic impedance). W=2.0 mm and g=s=1.0 mm, are used.

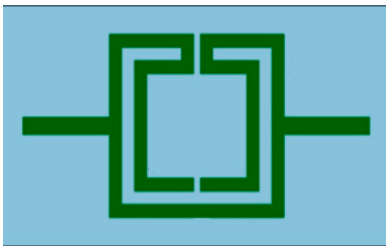

Figure 5. Example of microstrip filter based on an open Matryoshka geometry with two rings.

The 4 configurations, indicated in Table 1, have been numerically simulated in Ansoft HFSS [50]. Square rings are used (L_n=L_{xn}=L_{yn}). All the 4 configurations have the same average perimeter (P_N=178.00 mm).

Table 1. Physical characterization of Matryoshka geometries with two rings.

Configuration	L_1 [mm]	L_2 [mm]	L_{c1} [mm]
Config1	27.25	21.25	1.00
Config2	28.00	20.00	2.00
Config3	31.00	15.00	6.00
Config4	34.00	10.00	10.00

The simulated transmission coefficient of the four configurations is shown is Figure 6 for the open configuration and Figure 7 for the closed one.

 doi:10.20944/preprints202402.1017.v1

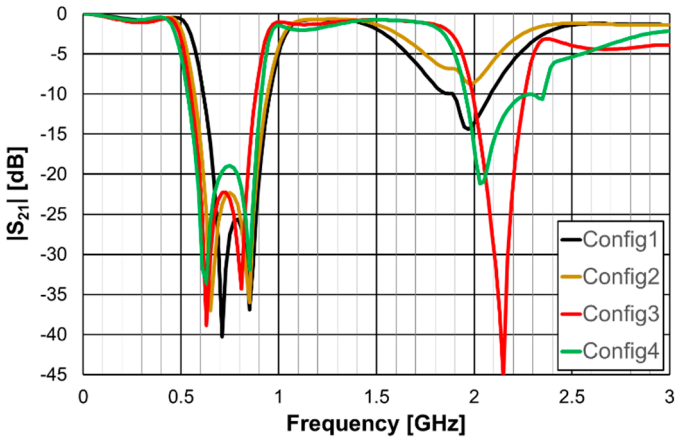

Figure 6. Simulated transmission coefficient of the open Matryoshka filters with constant length.

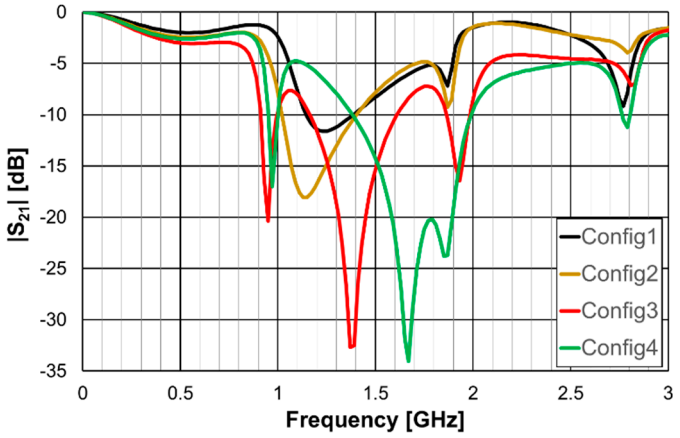

Figure 7. Simulated transmission coefficient of the closed Matryoshka filters with constant length.

As it can be concluded from Figure 6, the open configurations present adequate characteristics for a stopband filter, that is, high attenuation in the stopband, low attenuation in the passband, steep slope transition from passband to stopband (and vice-versa) and large bandwidth. However, that is not the case for the closed configurations (Figure 7). The open configuration provides a higher order filter because it offers two different resonance paths and the closed configurations just one. Moreover, as predicted, the open configurations have much lower first resonance frequencies. As it will be verified in the next sections, this conclusion is also obtained for the Matryoshka configurations used for other envisage applications (FSSs, antennas, sensors). Table 2 summarizes the characteristics of the open Matryoshka filter configurations.

For a single ring configuration, the effective length can be simply calculated as the average perimeter. However, for multiring Matryoshka configurations, there is coupling between the rings and there is not a simple physical interpretation of the effective length. To pre-design 2 rings configurations curve fitting has been used to obtain L_{ef} associated with the first two resonances [20].

$$L_{ef1} = 2[3(L_1 + L_2 - 4w) + L_c] \tag{8}$$

$$L_{ef2} = 2(3L_1 + 2L_2 - 10w) \tag{9}$$

 doi:10.20944/preprints202402.1017.v1

Table 2. Main characteristics of open Matryoshka filter configurations.

Configuration	fr_1 [GHz]		fr_2 [GHz]		f_0 [GHz]	BW* [%]
	Equation 2	Simulation	Equation 2	Simulation		
Config1	0.681	0.71	0.800	0.85	0.785	43.4
Config2	0.684	0.65	0.802	0.85	0.756	49.6
Config3	0.695	0.63	0.810	0.81	0.717	46.4
Config4	0.707	0.63	0.818	0.85	0.720	52.0

* Defined for a -10 dB reference level.

Equation 2 tends to provide better estimation of the first resonance frequency for intensive coupling (small Lc). Although the relative error can reach about 12% (for the first resonance of configuration 4), equation 2 is still very useful at the pre-design stage of these filters. These configurations provide miniaturized filters with very large bandwidth. The four configurations have different sizes for the rings and separation between them but, because they have the same perimeter, the stopband characteristics of the open configuration are very similar.

Microstrip filters based on open Matryoshka geometries with 2, 3 and 4 rings have also been simulated. The corresponding dimensions are indicated in Table 3. The previously indicated FR4 substrate, w=2.0 mm and g=s=1.0 mm, are used, again.

Table 3. Physical characterization of open Matryoshka geometries with 2, 3 and 4 rings.

Configuration	N	L_1 [mm]	L_2 [mm]	L_3 [mm]	L_4 [mm]	L_{c1} [mm]	L_{c2} [mm]	L_{c3} [mm]	P_N [mm]
Config5	2			NA	NA		NA	NA	210.00
Config6	3	32.00	24.00	16.00	NA	2.00	2.00	NA	268.00
Config7	4				8.00			2.00	294.00

The obtained $|S_{21}|$ results are shown in Figure 8.

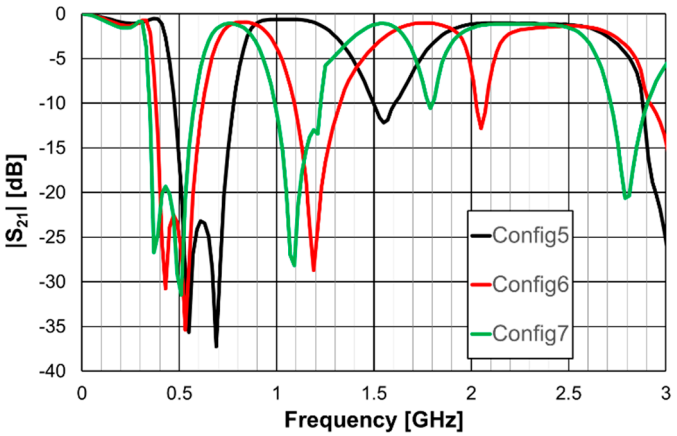

Figure 8. Simulated transmission coefficient of open Matryoshka filters with 2, 3 and 4 rings.

Table 4 contains the main simulation results associated with the first two resonances shown in Figure 8.

Table 4. Main characteristics of open Matryoshka filter configurations with 2, 3 and 4 rings.

Configuration	N	P_N [mm]	fr_1 [GHz]	fr_2 [GHz]	f_0 [GHz]	BW* [%]
Config5	2	210.0	0.55	0.69	0.627	48.7
Config6	3	268.0	0.43	0.53	0.501	48.4
Config7	4	294.0	0.37	0.51	0.462	50.3

* Defined for a -10 dB reference level.

 doi:10.20944/preprints202402.1017.v1

The use of more rings leads to the appearance of more resonances and, if the average perimeter increases, to a decrease of the frequency associated with the first two resonances.

The surface current density, on configuration 6, at the resonance frequencies and for frequencies between them, is shown in Figure 9.

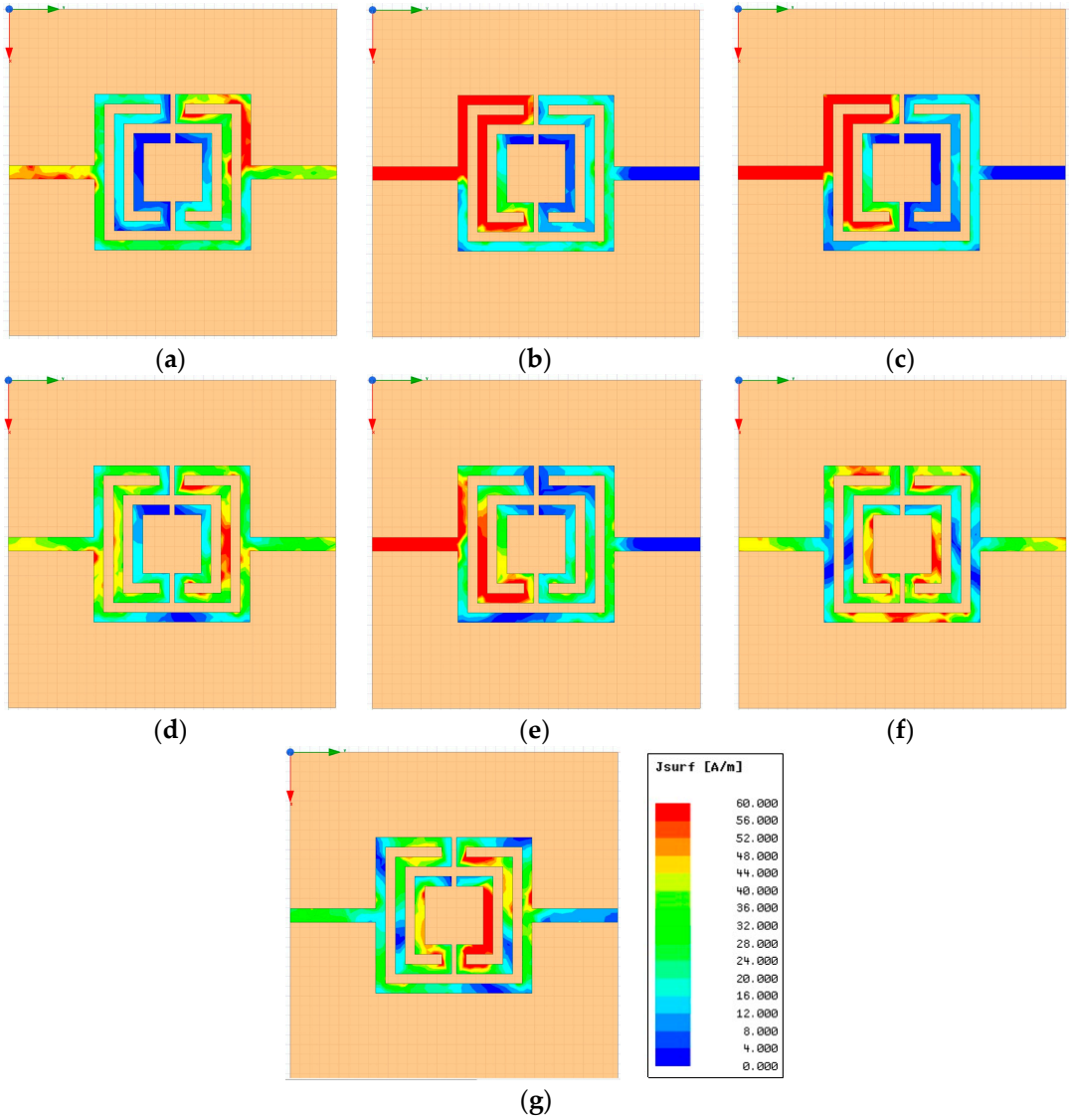

Figure 9. Simulated surface current density of the open Matryoshka filter with 3 rings (configuration 6). a) f=0.33 GHz, b) f=f_{r1}=0.43 GHz, c) f=f_{r2}=0.53 GHz, d) f=0.83 GHz, e) f=f_{r3}=1.19 GHz, f) f=1.79 GHz, g) f=f_{r4}=2.05 GHz.

There is a common pattern of the surface current distribution at the resonance frequencies. Being a stopband filter, there is no transmission at the resonance frequencies. In fact, for such frequencies (Figure 8b), c), e) and g)) the current at the output port is negligible, and the current at the input port is very strong due to a positive interference of the incident wave and the waves reflected at the two parallel paths, mostly if there is a good input impedance matching. For the frequencies between resonance frequencies, (Figure 8a), d) and f)) there is almost perfect transmission. It is also noticeable that the current magnitude on the inner rings increase as frequency goes up.

3. Examples of Application as FSS

The first application suggested for the Matryoshka geometry was as FSS [17,18]. This is quite logic since, at the time, there was already a strong and continued research activity in the topic FSS at GTEMA and FSS was already widely used in telecommunications systems. FSSs have been employed

 doi:10.20944/preprints202402.1017.v1

in radomes, absorbers, and dual-band antennas sub-reflectors systems [51,52]. A very important initial choice in the design of an FSS is the geometry of the unit-cell. Despite the variety of available geometries, with the rapid growing of wireless technologies, telecommunication system requirements impose a continuing challenge to meet characteristics as miniaturization, multiband operation, polarization independence, etc.

3.1. Closed Matryoshka FSSs

In [17,18] the closed square Matryoshka geometry with two rings, shown in Figure 10, is introduced. A 0.97 mm thick FR4 substrate with ε_r=4.4 and tanδ=0.02 is used. The dimensions (in mm) of two configuration are indicated in Table 5, and Wx=Wy=24.0 mm.

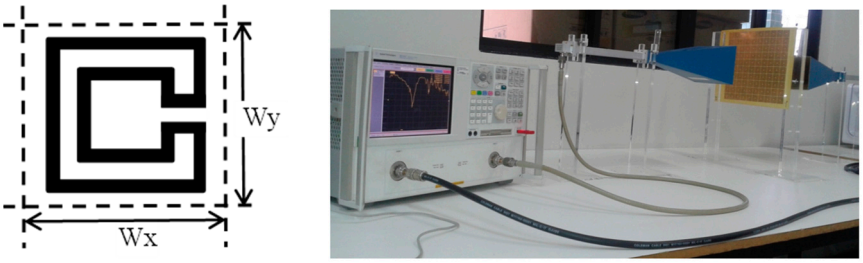

(**a**) (**b**)

Figure 10. Closed Matryoshka FSS. a) Unit-cell geometry. b) Photo of the prototype with 10x10 unit-cells and measurement setup.

Table 5. Dimensions of the closed square Matryoshka geometry with two rings.

Configuration	L_1	L_2	L_{c1}	w	g	P_2 [mm]
Config1	22.0	12.0	3.5	1.5	1.0	129.0
Config2		7.0	6.0			114.0

Using equations 1, 4, and 5 and the procedure proposed in [17,18] to estimate L_{ef} and ε_{ref}, the initial dimensions of the Matryoshka unit-cell, fulfilling the specifications, can be obtained. L_{ef} depends on the polarization considered. Usually the two orthogonal linear polarization (vertical-V and horizontal-H) are employed. The use of a numerical simulator can then provide the necessary optimization.

The simulation and experimental transmission coefficient results, obtained for the configuration 1, are shown in Figure 11. The simulation results correspond to an infinite FSS (Floquet boundary conditions [51,52]). The horn antennas, available at the time, only allowed measurements above 4.5 GHz.

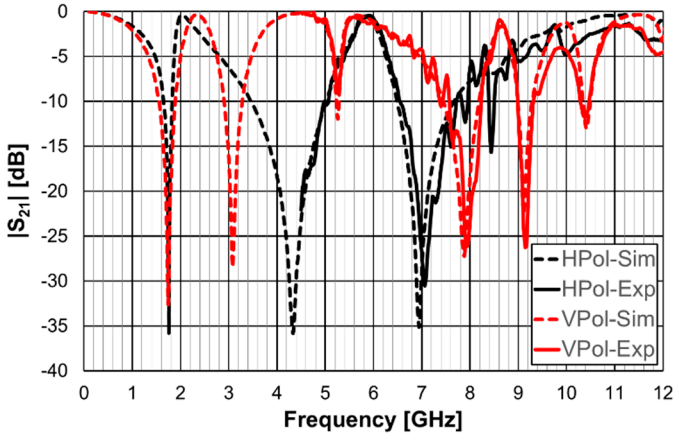

Figure 11. Simulated and experimental $|S_{21}|$ results for configuration 1.

Preprints.org (www.preprints.org) | NOT PEER-REVIEWED | Posted: 19 February 2024 doi:10.20944/preprints202402.1017.v1

A general good agreement is obtained between simulation and experimental results. The ripple in the experimental results is caused by the reflections on the objects present in the non-anechoic environment of the laboratory. The transmission coefficient results depend on the polarization (horizontal-H or vertical-V) of the incident electric field. However, the first resonance frequency is the same for both polarizations (1.75 GHz), but the -10 dB bandwidth is larger for the vertical polarization (19.8% and 10.0%).

The simulation results obtained for the two configurations are compared in Figure 12.

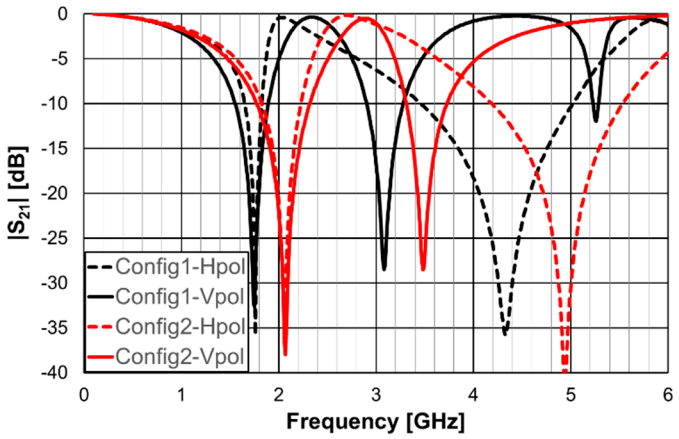

Figure 12. Comparison of the simulated $|S_{21}|$ results for configurations 1 and 2.

Although both configurations have the same external ring dimensions, configuration 1 has a larger L_{ef} and consequently its resonance frequencies are lower. For instance, f_{res11}=1.75 GHz and f_{res12}=2.06 GHz. Configuration 2 has a much larger bandwidth for both polarizations. For the vertical polarization BW_1=19.8% whereas BW_2=26.7%. The dimensions of the internal ring can be used to fine tune de FSS and to control the bandwidth.

3.2. Open Matryoshka FSSs

In [19,32] the open Matryoshka geometry is introduced, reducing the first resonance frequency to approximately half, when compared to the closed Matryoshka geometry FSS, previously analyzed. It is interesting to compare, now for application in FSSs, the simple rings, with closed and open Matryoshka geometries, as shown in Figure 13. Again, a 0.97 mm thick FR4 substrate with ε_r=4.4 and tanδ=0.02 is used. A unit-cell with size Wx=Wy=24.0 mm, L_1=22.0 mm, L_2=12 mm, L_c=3.5 mm, w=1.5 mm and g=s=1.0 mm is chosen.

(**a**) (**b**) (**c**)

Figure 13. FSS square unit-cells with two square rings. a) Simple rings. b) Closed Matryoshka geometry. c) Open Matryoshka geometry.

The simulated $|S_{21}|$ results are shown in Figure 14 for horizontal polarization, and in Figure 15 for vertical polarization.

Preprints.org (www.preprints.org) | NOT PEER-REVIEWED | Posted: 19 February 2024 doi:10.20944/preprints202402.1017.v1

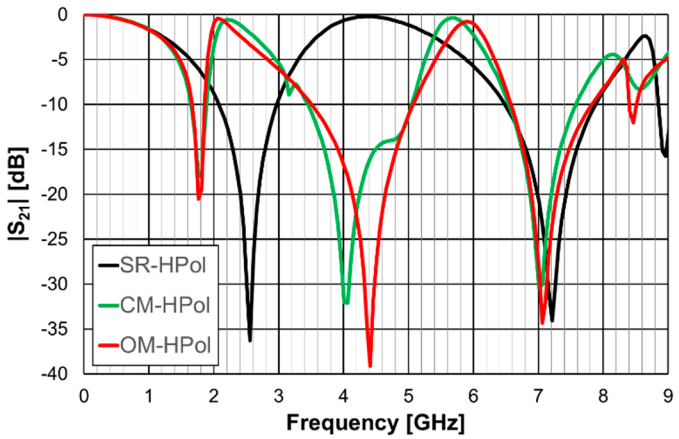

Figure 14. Simulated $|S_{21}|$ results of the simple rings (SR), closed Matryoshka (CM) and open Matryoshka (OM), for horizontal polarization (HPol).

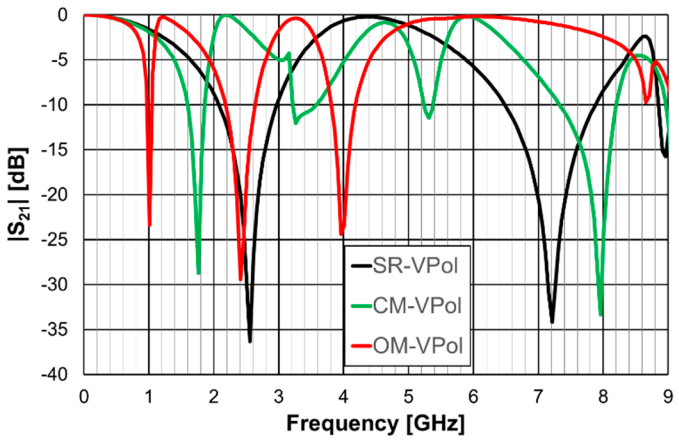

Figure 15. Simulated $|S_{21}|$ results of the simple rings (SR), closed Matryoshka (CM) and open Matryoshka (OM), for vertical polarization (VPol).

The simple rings configuration is physically symmetric and therefore its response is the same for the horizontal and vertical polarizations. That is also the case for the closed Matryoshka configuration, but only for the first resonance. However, the open Matryoshka configuration has completely different responses for the two polarizations. Although the 3 configurations occupy the same area, the two unit-cell with Matryoshka geometry provide much lower first resonance frequencies, especially for vertical polarization. The results associated with the first resonance are summarized in Table 6.

The FSS with open Matryoshka geometry provides a remarkable reduction of the first resonance frequency, especially for vertical polarization, when compared with the closed configuration (43%) and with the simple rings (61%). However, there a substantial reduction of the bandwidth.

Table 6. Summary of the first resonance results for the square ring (SR) unit-cells FSSs with simple rings and close (CM) and open (OM) Matryoshka geometries.

Unit-cell geometry	First resonance frequency [GHz]		Bandwidth* [%]	
	HPol	VPol	HPol	VPol
SR	2.56	2.56	35.4	35.4
CM	1.78	1.78	13.6	15.3
OM	1.78	1.01	10.9	8.1

* Defined for a -10 dB reference level.

 doi:10.20944/preprints202402.1017.v1

The simulation results for the open Matryoshka configuration were validated with experimental results, as shown in Figure 16.

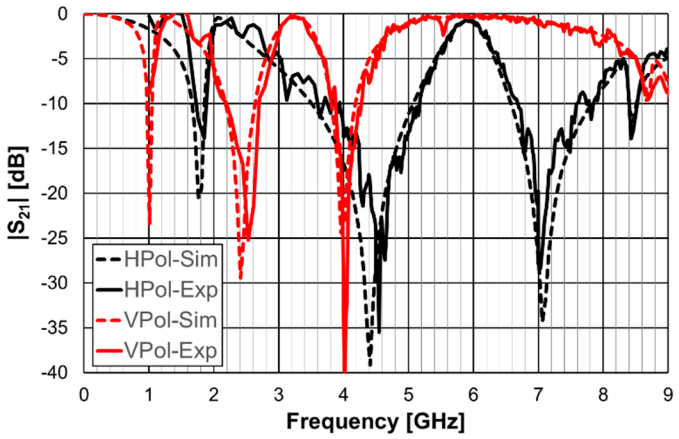

Figure 16. Comparison of simulated and experimental $|S_{21}|$ results of the open Matryoshka, for horizontal and vertical polarizations.

More rings can be used to increase que effective length and therefore, further reduce the first resonance frequency, increase the number of resonances, and provide a fine tune control of the resonances and of the bandwidth [19,32]. To confirm these conclusions, an FSS with open Matryoshka unit-cell with 3 rings was designed, fabricated, and tested. Again, a 0.97 mm thick FR4 substrate with ε_r=4.4 and tanδ=0.02 was used. A unit-cell with size Wx=Wy=24.0 mm, L1=22.0 mm, Lc1=Lc2=2.25 mm, L2=14.5 mm, L3=7.0 mm w=1.5 mm and g=s=1.0 mm was chosen. Photos of the prototype and of the experimental setup are shown in Figure 17.

(**a**) (**b**)

Figure 17. Photo of the FSS test procedure. a) Prototype. b) Experimental setup.

Simulation and experimental results of the 3 rings open Matryoshka geometry for vertical and horizontal polarizations are shown in Figure 18. The experimental results could only be measured starting at 1 GHz. There is a general good agreement between simulation and experimental results. As mentioned before, and as it can be verified in Figure 17b, the ripple in the experimental results is caused by the reflections on the objects present in the non-anechoic environment of the laboratory.

Preprints.org (www.preprints.org) | NOT PEER-REVIEWED | Posted: 19 February 2024 doi:10.20944/preprints202402.1017.v1

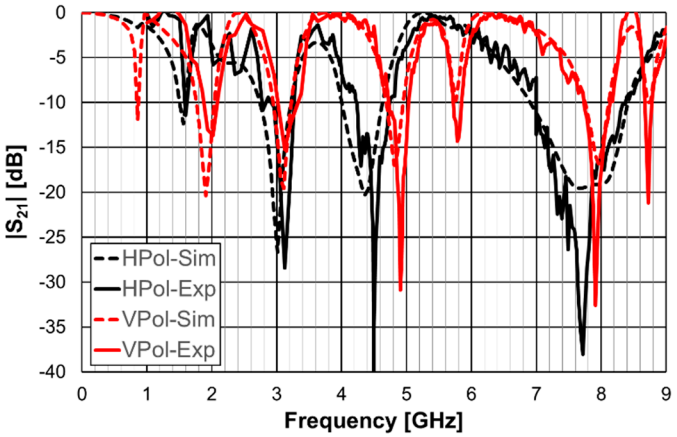

Figure 18. Comparison of simulated and experimental $|S_{21}|$ results of the open Matryoshka with 3 rings, for horizontal and vertical polarizations.

The simulation results of the FSS with open Matryoshka unit-cells with 2 and 3 rings are summarized in Table 7.

Table 7. Summary of the simulation results of the FSS with open Matryoshka unit-cells with 2 and 3 rings.

N	Area	f_{r1} [GHz]		Bandwidth* [%]		f_{r2} [GHz]		f_{r3} [GHz]	
	[mm²]	HPol	VPol	HPol	VPol	HPol	VPol	HPol	VPol
2	22x22	1.78	1.01	10.9	8.1	4.36	2.41	7.66	3.96
3		1.56	0.86	5.9	2.9	3.01	1.91	4.36	3.11

* Defined for a -10 dB reference level.

It is confirmed that, for the same dimension of the external ring the increase of the number of rings (2 to 3) provides a reduction of the first resonance frequency, an increase of the number of resonances, and fine tune control of the resonances. However, a reduction of the bandwidth is verified.

3.3. Polarization Independent FSSs

To overcome the inconvenient polarization dependence, analyzed in the previous section, a new configuration of the Matryoshka geometry is proposed in [21,36]. As shown in Figure 19, this new type of configuration has been conceived as an evolution from the simple circular ring keeping the main Matryoshka characteristics, that is, the area occupied is defined by the external ring only and more rings can be added internally maintaining electrical continuity. The physical characterization of the circular Matryoshka geometry is defined in Figure 20.

FSS unit-cells with the 3 geometries shown in Figure 19 were designed, fabricated ant tested [21,36]. A 0.762 mm thick FR4 substrate with ε_r=4.4 and tanδ=0.02 is used. An FSS with 10x10 unit-cells with size Wx=Wy=20.0 mm and w=g=0.8 mm is chosen. The radius of the unit-cells' rings are indicated in Table 8. The radius reduction rate is maintained from ring to ring.

(**a**) (**b**) (**c**)

Preprints.org (www.preprints.org) | NOT PEER-REVIEWED | Posted: 19 February 2024 doi:10.20944/preprints202402.1017.v1

Figure 19. Evolution from a simple circular ring to a circular multiring Matryoshka geometry. a) Simple circular ring. b) Circular Matryoshka geometry with 3 rings. c) Circular Matryoshka geometry with 5 rings.

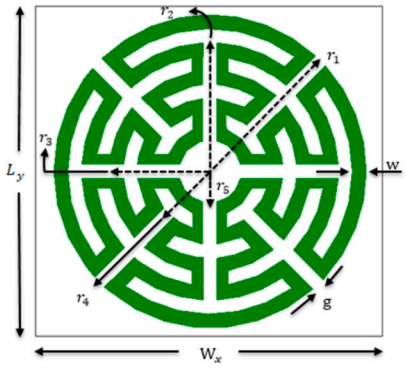

Figure 20. Definition of the physical parameters of an FSS unit-cell with circular multiring Matryoshka geometry.

Table 8. Radius of the circular Matryoshka unit-cells.

Configuration	Number of rings	r_1 [mm]	r_2 [mm]	r_3 [mm]	r_4 [mm]	r_5 [mm]
FSS1	1	9.0	7.4	5.8	NA	
FSS2	3				4.2	NA
FSS3	5					2.6

As the FSSs are horizontally and vertically symmetric, they are polarization independent. Therefore, for these three cases, only results obtained for vertical polarization are shown. An important characteristic of an FSS is its sensitivity to the angle of the incident electromagnetic wave. Four angles of incidence were considered, from normal incidence (θ=0) to θ=45º, with a 15º interval.

In [21,36] the formulas indicated in equations 10 to 12 are proposed to estimate the first resonance frequency of the FSS with 1, 3 and 5 rings, respectively. These formulas were used to specify the radius of the 3 configurations at the initial stage of the design procedure.

$$f_{rFSS1} = \frac{3x10^8}{2\pi r_1\sqrt{\varepsilon_{ref}}} \tag{10}$$

$$f_{rFSS2} = \frac{3x10^8}{2\pi(r_1 + r_3)\sqrt{\varepsilon_{ref}}} \tag{11}$$

$$f_{rFSS3} = \frac{3x10^8}{2\pi(r_1 + r_3 + r_5)\sqrt{\varepsilon_{ref}}} \tag{12}$$

ε_{ref} is the effective relative permittivity of the equivalent homogeneous structure [21,36].

The prototypes, shown in Figure 21, were fabricated, and measured using the setup shown in Figure 22.

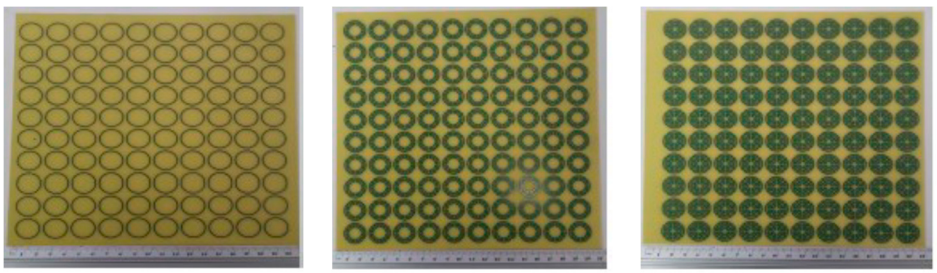

(**a**) (**b**) (**c**)

 doi:10.20944/preprints202402.1017.v1

Figure 21. Prototypes of the FSSs with circular Matryoshka unit-cells. a) FSS1 b) FSS2. c) FSS3.

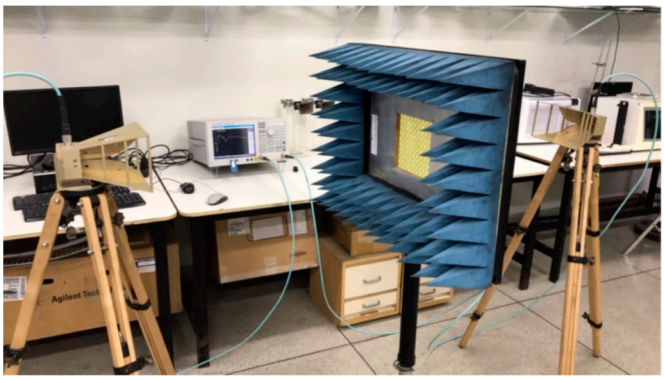

Figure 22. Setup for the measurement of the FSS prototypes with circular Matryoshka unit-cells.

The simulation and experimental results obtained for the transmission coefficient of the three prototypes are shown in Figures 23–25. The simulation results for the four different incident angles are very similar and, therefore, for the sake of clarity, only one curve is represented.

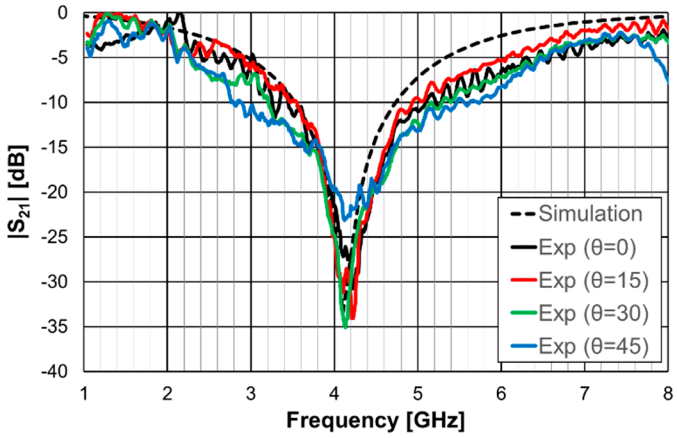

Figure 23. Comparison of simulated and experimental $|S_{21}|$ results of FSS1 prototype.

There is a good agreement between numerical simulations and experimental results, for the three prototypes. In general, the measured results are below the simulation ones. This difference is about 5 dB, in average, and tend to increase as the oblique angle of incidence increases. This effect may be caused by the finite size of the window used in the measurement setup (Figure 22).

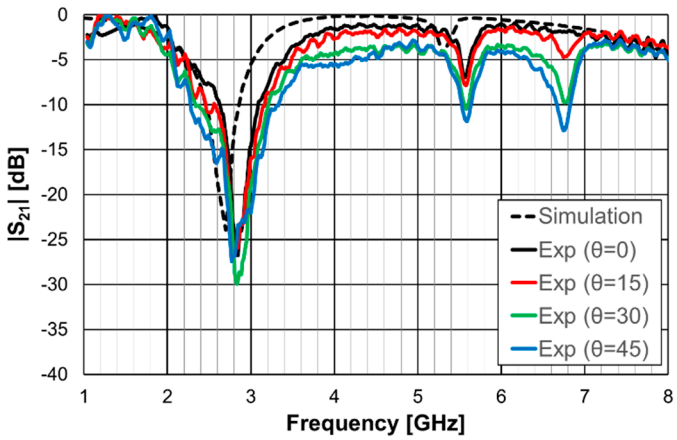

Preprints.org (www.preprints.org) | NOT PEER-REVIEWED | Posted: 19 February 2024 doi:10.20944/preprints202402.1017.v1

Figure 24. Comparison of simulated and experimental $|S_{21}|$ results of FSS2 prototype.

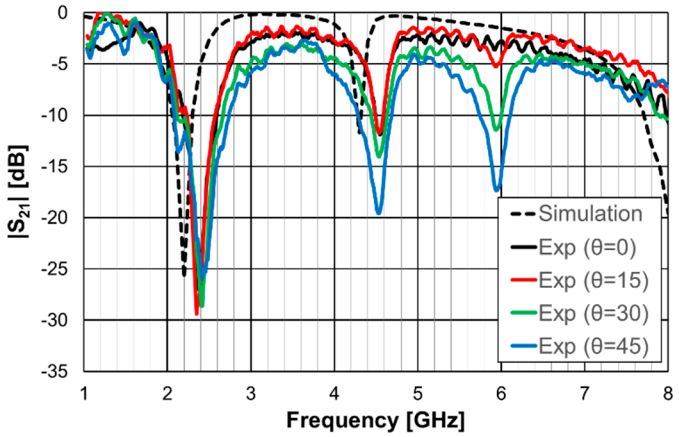

Figure 25. Comparison of simulated and experimental $|S_{21}|$ results of FSS3 prototype.

As the perimeter of the FSS unit-cell increases with the number of rings more resonances appear. The results, for the first resonance frequency are compared in Table 9.

Table 9. Comparison of first resonance frequencies of the FSSs prototypes.

Configuration	Number of rings	First resonance frequency [GHz]					
		Estimation	Simulation	Experimental			
				Θ=0	Θ=15º	Θ=30º	Θ=45º
FSS1	1	4.45[1]	4.10	4.224	4.211	4.133	4.120
FSS2	3	2.71[2]	2.70	2.846	2.833	2.833	2.768
FSS3	5	2.30[3]	2.20	2.378	2.352	2.404	2.417

[1] Equation 10 [2] Equation 11 [3] Equation 12.

There is a good agreement between numerical simulation and experimental results. Moreover, also the estimation provided by equations 10, 11 and 12 is accurate enough for the initial stage of the design (relative error below 5%). It is clear that the three prototypes have low sensitivity from the inclination angle and that there is a remarkable reduction in the first resonance frequency as the number of rings increase (44% from FSS1 to FSS3).

Recently a polarization insensitive miniaturized multiband FSS with Matryoshka geometry elements was proposed [42]. From an initial polarization sensitive unit-cell with a single element there is an evolution to a combination of four orthogonal of such unit-cells (Figure 26).

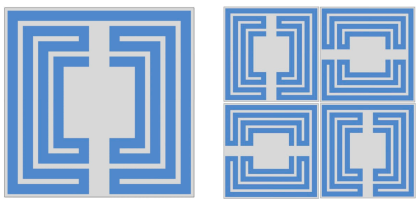

(**a**) (**b**)

Figure 26. Matryoshka unit-cells proposed in [42]. a) Single element b) Combination of four orthogonal elements.

The simulation results for the transmission coefficient of the two Matryoshka unit-cells, for normal incidence (θ=0), are shown in Figures 27 and 28.

Preprints.org (www.preprints.org) | NOT PEER-REVIEWED | Posted: 19 February 2024 doi:10.20944/preprints202402.1017.v1

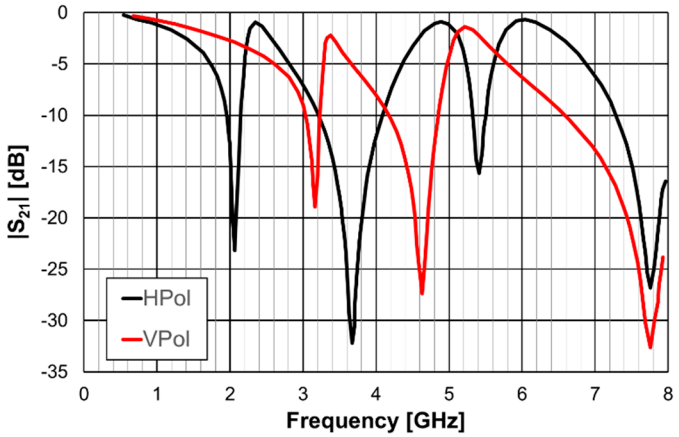

Figure 27. $|S_{21}|$ simulation results of the FSS with the single element Matryoshka unit-cell.

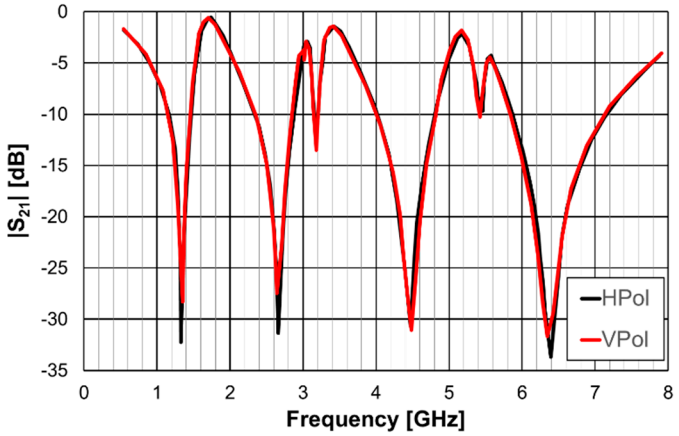

Figure 28. $|S_{21}|$ simulation results of the FSS with the four orthogonal Matryoshka elements unit-cell.

The single element unit-cell has a strong polarization dependence, but the four orthogonal elements unit-cell is almost perfectly polarization independent. Moreover, from the results presented in Figures 29 and 30 it can be concluded that the new 4 elements arrangement also provides low sensitivity to the angle of incidence. For horizontal polarization the curves for θ=0, θ=20° and θ=40° are almost coincident, only the curve for θ=60° is slightly different. For vertical polarization the situation is almost the same, but both the curves for θ=40° and for θ=60° are slightly different from the other two.

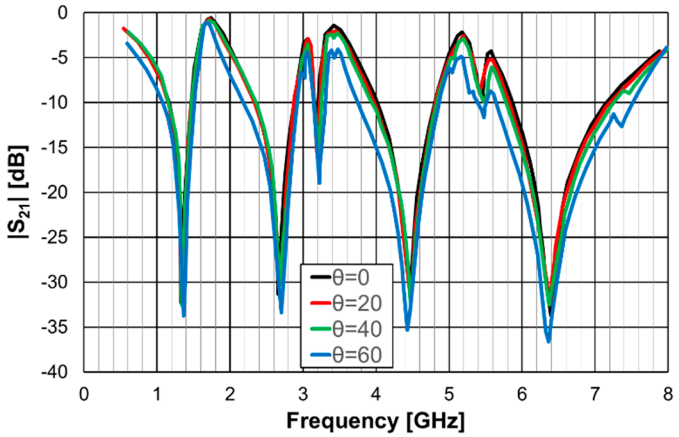

Preprints.org (www.preprints.org) | NOT PEER-REVIEWED | Posted: 19 February 2024 doi:10.20944/preprints202402.1017.v1

Figure 29. $|S_{21}|$ simulation results of the FSS with the four orthogonal Matryoshka elements unit-cell for horizontal polarization.

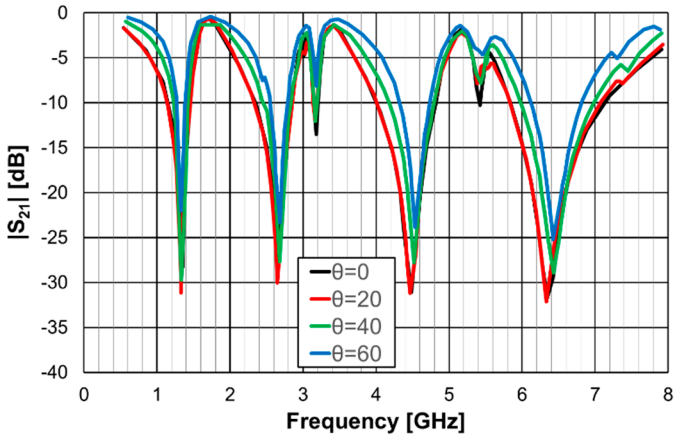

Figure 30. $|S_{21}|$ simulation results of the FSS with the four orthogonal Matryoshka elements unit-cell for vertical polarization.

3.4. Combination of an FSS with Dipoles

One of the advantages of the Matryoshka geometry is that it can be combined with other geometries, to obtain an FSS with low coupling between the fields of each geometry, allowing to control the respective frequency responses. This is particularly interesting for the design of multiband FSS. In [23,27] cross-dipoles and Matryoshka geometries are combined to achieve a polarization independent triple-band FSS. The combined geometries are shown in Figure 31. The prototype, shown in Figure 32, was fabricated, and characterized.

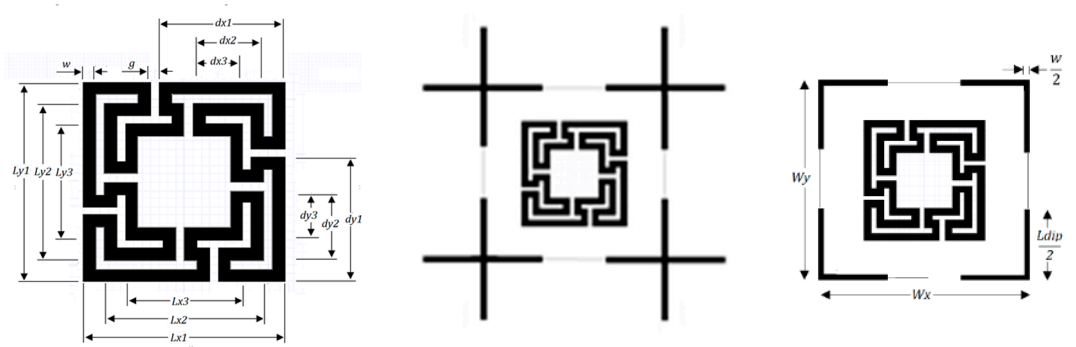

Figure 31. Combination of a Matryoshka geometry with cross-dipoles to form an FSS. a) Matryoshka geometry. b) Combination of Matryoshka with cross-dipoles. c) FSS unit-cell.

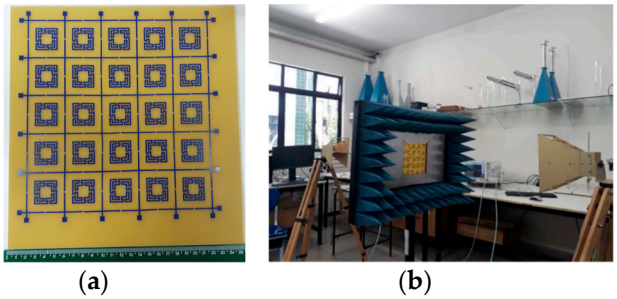

Figure 32. Photos of the FSS with combination of the Matryoshka geometry with cross-dipoles. a) Prototype. b) Experimental setup.

Preprints.org (www.preprints.org) | NOT PEER-REVIEWED | Posted: 19 February 2024 doi:10.20944/preprints202402.1017.v1

In [23], a 1.6 mm thick FR4 substrate with ε_r=4.4 and tanδ=0.02 is used. The simulation results shown in Figure 33 correspond to an FSS with 5x5 unit-cells with size Wx=Wy=40.0 mm, w=1.5 mm and g=1.0 mm. Moreover, $L_{x1}=L_{y1}$=24.0 mm, $L_{x2}=L_{y2}$=19.0 mm $L_{x3}=L_{y3}$=14.0 mm, $d_{x1}=d_{y1}$=15.0 mm, $d_{x2}=d_{y2}$=8.5 mm $d_{x3}=d_{y3}$=6.0 mm, and L_{dip}=39.0 mm. Three resonances can be observed (f_{r1}=1.81 GHz, f_{r2}=2.43 GHz, and f_{r3}=3.19 GHz). They correspond to the superposition of the first and second resonances of the Matryoshka geometry (f_{r1}=1.82 GHz and f_{r2}=3.18 GHz)with the first resonance of the cross-dipoles (f_{r1}=2.46 GHz). The three resonances can be controlled separately which is a very interesting feature that adds flexibility in the design for different potential applications. For instance, it is possible to design the dipole so that its first resonance frequency is close to one of the resonance frequencies of the Matryoshka geometry (first or second). By doing this an increase of the bandwidth of the combined resonances can be obtained. Numerical simulation results are compared with experimental results, obtained for different angles of incidence, in Figure 34.

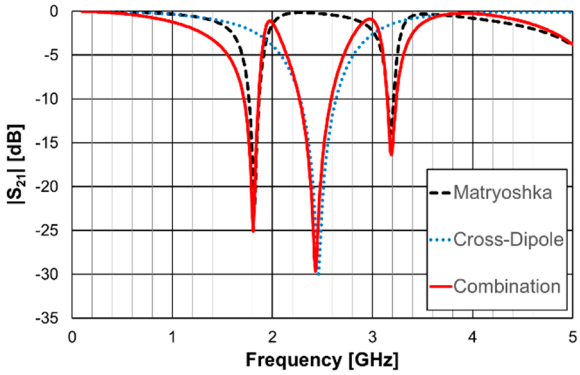

Figure 33. $|S_{21}|$ response of an FSS for the Matryoshka geometry, the cross-dipoles, and the combination of the two.

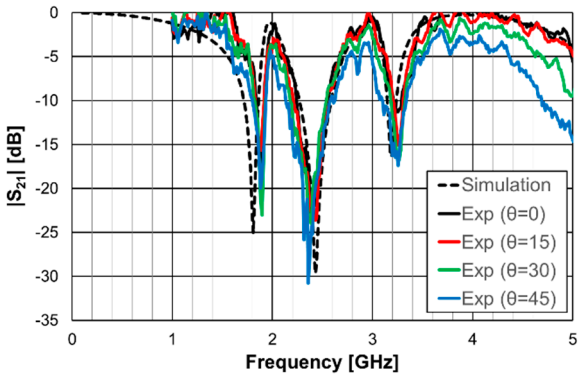

Figure 34. Comparison of $|S_{21}|$ simulation and experimental results for the FSS combination of the Matryoshka geometry with the cross-dipoles.

The simulation results for the four different incident angles are very similar and, therefore, for the sake of clarity, only one curve is represented. There is a general good agreement between simulation and experimental results which validates the design procedure. Moreover, the angular stability is confirmed. The discrepancies observed may be caused by the finite size of the window used in the measurement setup (Figure 32b).

3.5. Complimentary FSSs

The Matryoshka geometry, described in the previous section, is also used in its complementary form [24,39]. The FSS unit-cell is obtained as described in Figure 35.

Preprints.org (www.preprints.org) | NOT PEER-REVIEWED | Posted: 19 February 2024 doi:10.20944/preprints202402.1017.v1

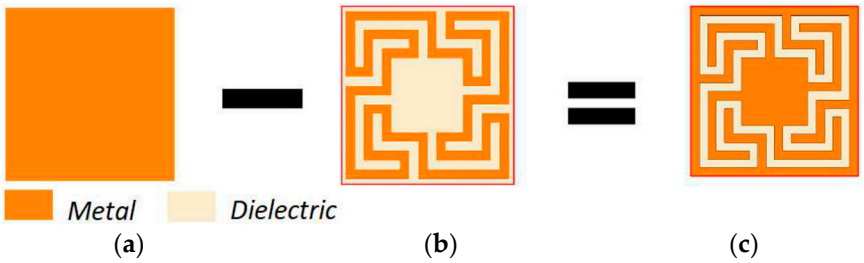

Figure 35. Complementary form of FSS Matryoshka geometry unit-cell. a) Metal patch. b) Metal Matryoshka geometry. c) Complementary Matryoshka geometry.

It is shown in the previous section that the Matryoshka geometry with metal strips has a stopband response associated with its resonances. The complimentary Matryoshka geometry has a passband behavior. Two prototypes of these complimentary Matryoshka configurations with 9x9 unit-cells, each cell with 22.4x22.4 mm², were designed, fabricated, and tested [24,39]. A 1.6 mm thick FR4 substrate with ε_r=4.4 and tanδ=0.02 and w=g=1.0 mm is used. The simulation results shown in Figure 36 correspond to FSS1 ($L_{x1}=L_{y1}$=20.4 mm, $L_{x2}=L_{y2}$=16.4 mm $L_{x3}=L_{y3}$=12.4 mm, $d_{x1}=d_{y1}$=11.4 mm, $d_{x2}=d_{y2}$=7.4 mm $d_{x3}=d_{y3}$=5.5 mm) and FSS2 ($L_{x1}=L_{y1}$=15.4 mm, $L_{x2}=L_{y2}$=11.4 mm $L_{x3}=L_{y3}$=7.4 mm, $d_{x1}=d_{y1}$=9.0 mm, $d_{x2}=d_{y2}$=5.0 mm $d_{x3}=d_{y3}$=3.0 mm). These dimensions were calculated using the design formulas proposed in [24] to provide passbands centered at 1.5 GHz and 3.5 GHz for FSS1 and 2.5 GHz and 5.1 GHz for FSS2, and a stopband centered at 2.45 GHz for FSS1 and 3.5 GHz for FSS2. Photos of these complimentary FSS prototypes era shown in Figure 36.

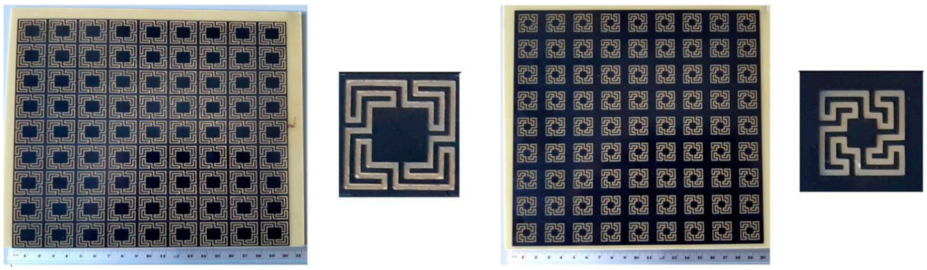

Figure 36. Photos of the prototypes of the complimentary Matryoshka configurations FSS1 and FSS2. a) FSS1. b) FSS2.

The results shown in Figure 37 demonstrate that it is possible to adjust the range of the stopbands and passbands according to the specifications.

As shown in the previous section this Matryoshka configuration has very good angular stability. From the results presented in Figures 38 and 39 it can be also concluded that the complimentary Matryoshka configuration presents the same good angular stability.

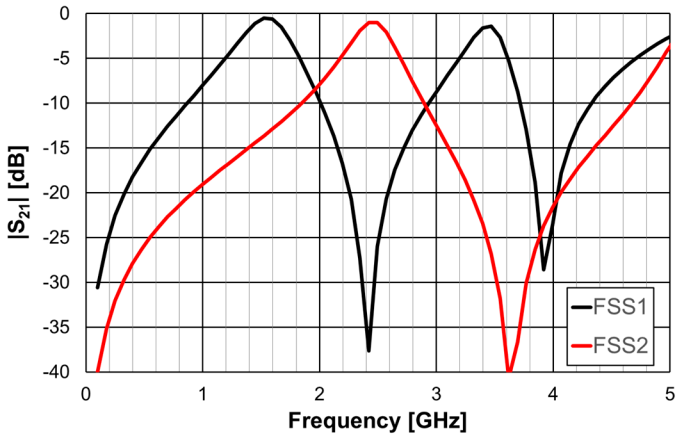

Preprints.org (www.preprints.org) | NOT PEER-REVIEWED | Posted: 19 February 2024 doi:10.20944/preprints202402.1017.v1

Figure 37. |S21| simulation results of the complimentary Matryoshka configurations FSS1 and FSS2.

The simulation results for the four different incident angles are very similar and, therefore, for the sake of clarity, only one curve is represented. Taking into account that the experimental results were obtained in a simple non-anechoic room, there is a good agreement between numerical simulation and experimental results. The resonance and antiresonance frequencies are confirmed experimentally with relative error differences below 4.5% [24].

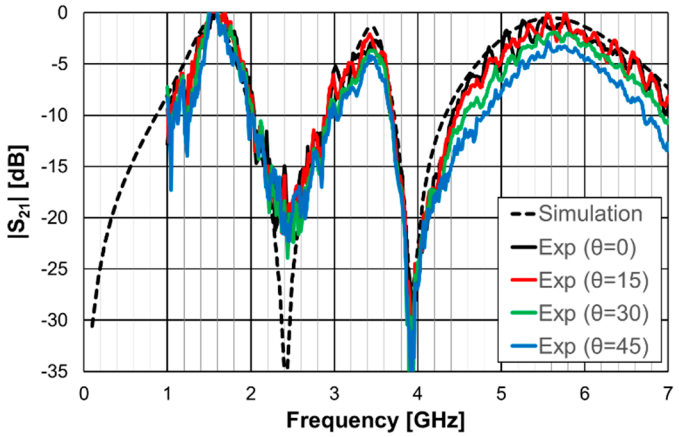

Figure 38. Comparison of |S21| simulation and experimental results for the FSS1.

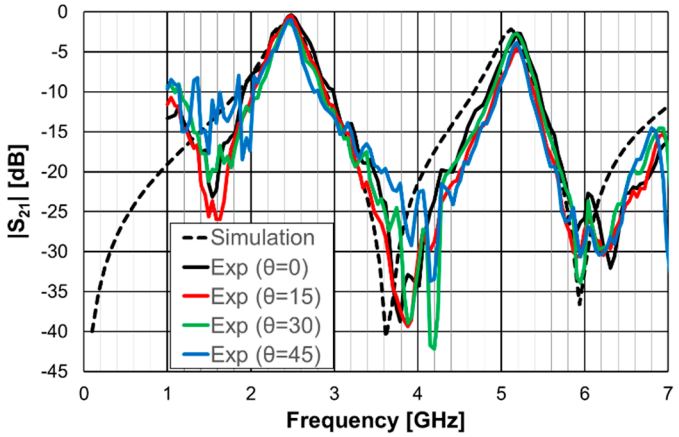

Figure 39. Comparison of |S21| simulation and experimental results for the FSS2.

3.6. Reconfigurable FSSs

For some applications, reconfigurability is a very attractive feature for an FSS. In this case, combined geometries can be useful. Adding a PIN diode between the vertical dipoles of the FSS presented in [23], and analyzed in section 3.4, a reconfigurable FSS (RFSS) is obtained, as described in [27]. Additionally, as shown in Figure 40, a RF inductor was added between the horizontal dipoles to act as an RF choke [49]. The RFSS prototype, shown in Figure 40c, was fabricated, and characterized [27].

 doi:10.20944/preprints202402.1017.v1

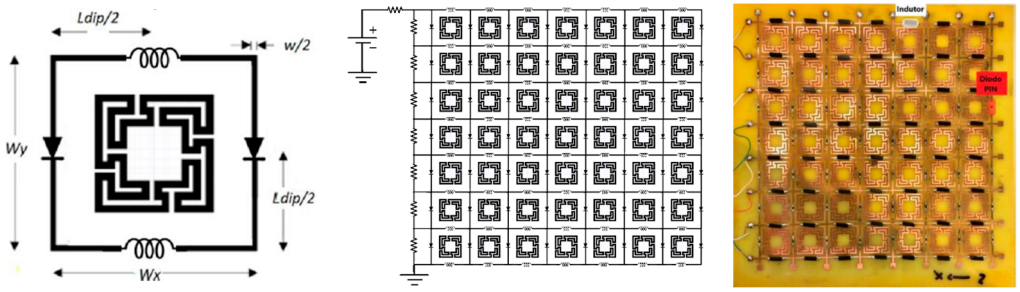

(a) (b) (c)

Figure 40. RFSS with Matryoshka geometry. a) Unit-cell. b) 7x7 configuration. c) Prototype.

A 1.6 mm thick FR4 substrate with ε_r=4.4 and tanδ=0.02 is used. The prototype shown in Figure 40c corresponds to an FSS with 7x7 unit-cells with size W_x=W_y=30.0 mm, w=1.5 mm and g=1.0 mm. Moreover, L_{x1}=L_{y1}=24.0 mm, L_{x2}=L_{y2}=19.0 mm L_{x3}=L_{y3}=14.0 mm, d_{x1}=d_{y1}=15.0 mm, d_{x2}=d_{y2}=8.5 mm d_{x3}=d_{y3}=6.0 mm, and L_{dip}=29.0 mm. Numerical simulation and measured results are presented in Figures 41 to 45. Figure 41 corresponds to unit-cells without PIN diodes and without inductors. These results serve as a reference. Figure 42 corresponds to unit-cells with PIN diodes but without inductors. Figures 43–45 correspond to unit-cells with both PIN diodes and inductors.

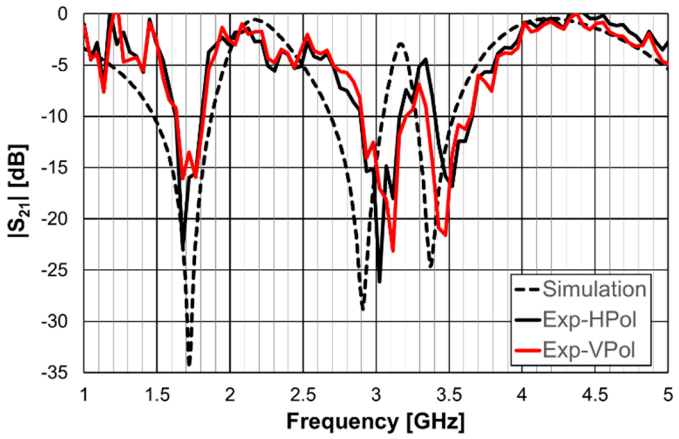

Figure 41. $|S_{21}|$ response of the FSS without PIN diodes and without inductors.

In Figure 41 the simulation results for the horizontal and vertical polarization are identical, for the sake of clarity only one curve is represented. There is a reasonable agreement between simulation and experimental results. The experimental second and third resonances are substantially deviated from the simulations. The difference may reach 6.6% and is mainly caused by the non-anechoic environment of the laboratory and eventual fabrication inaccuracies.

In Figure 42, the agreement between numerical simulation and experimental results is good, except for the second resonance and horizontal polarization (7% relative error). In addition to the already mentioned general error causes (non-anechoic environment and fabrication inaccuracies) there must be some other problem not detected. However, as this configuration is just an intermediate step and new prototypes would be fabricated for the next steps the work was continued.

Preprints.org (www.preprints.org) | NOT PEER-REVIEWED | Posted: 19 February 2024 doi:10.20944/preprints202402.1017.v1

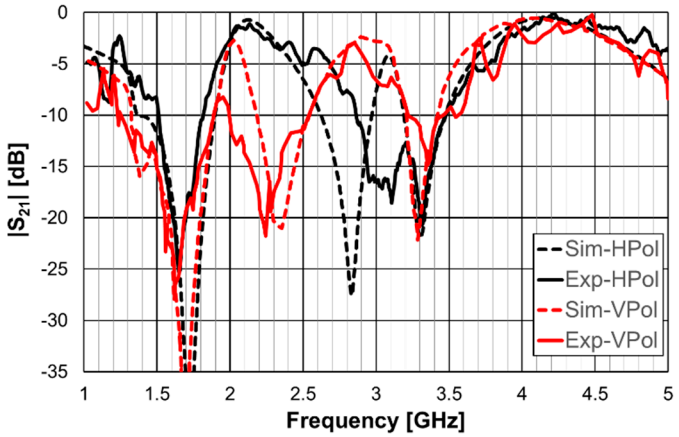

Figure 42. |S21| response of the FSS with PIN diodes but without inductors.

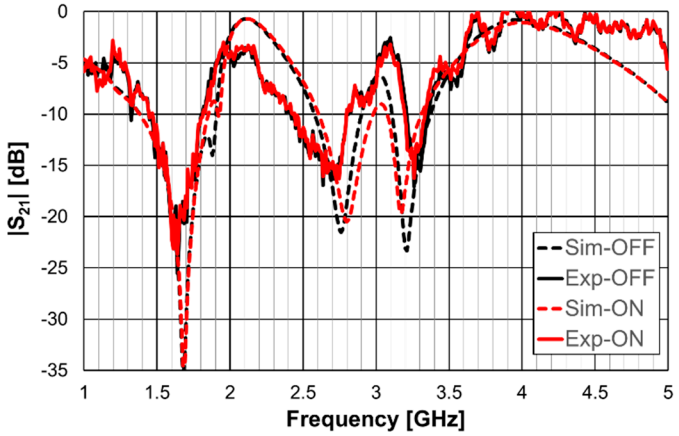

Figure 43. |S21| response of the FSS with PIN diodes and inductors, for horizontal polarization.

The results shown in Figure 43 indicate that, as expected, the state of the diode does not affect the horizontal polarization. Moreover, the problem associated with the second resonance frequency, detected in Figure 42, disappeared. The relative error for the second resonance frequency is now only about 4%. It is, therefore, verified the need to use the inductors. In Figure 44, a good agreement between simulation and experimental results is verified, for both OFF and ON states.

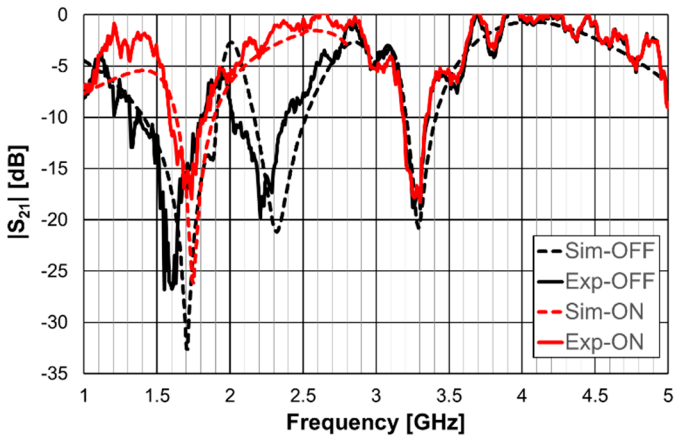

Figure 44. |S21| response of the FSS with PIN diodes and inductors, for vertical polarization.

 doi:10.20944/preprints202402.1017.v1

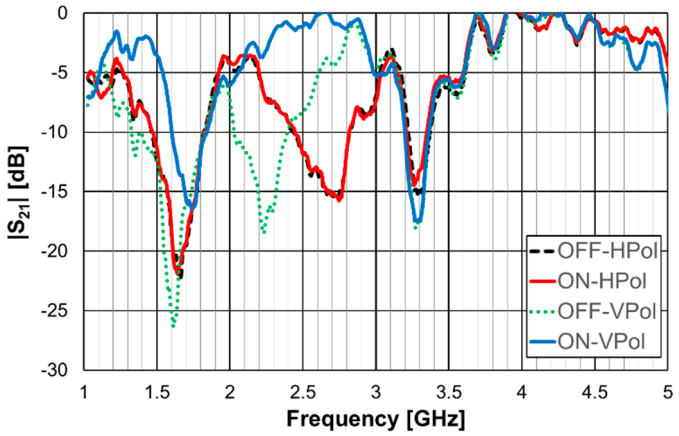

Figure 45. $|S_{21}|$ response of the FSS with PIN diodes and inductors, for ON and OFF PIN states.

As it can be concluded from the results presented in Figure 45, for vertical polarization, the reconfiguration of the FSS is effective, with a reconfigurable bandwidth of 0.37 GHz (17%), from 2.03 GHz to 2.40 GHz, with at least 10 dB of difference between OFF and ON bias states of the diodes.

4. Examples of Application as Filter

Providing access to telecommunication networks in the most diverse locations, with quality of service and without losing mobility, poses major challenges for manufacturers of mobile equipment and infrastructures. In both cases, filters play a fundamental role, separating the desired signals from the unwanted ones. Telecommunication systems require filters with operating conditions that are increasingly challenging in terms of frequency response, in addition to low cost, weight and volume (miniaturization). In this sense, new microwave filter configurations have been developed [53,54]. To meet these requirements, planar filters are widely used. Planar filters can be viewed as resonators, lumped or quasi-lumped, for which the resonance frequency is determined by the geometry [49,55]. Aiming to take advantage of the characteristics observed for the Matryoshka geometry when used in FSSs (miniaturization and multiband operation), filters based on Matryoshka geometries, were introduced in [20,26].

4.1. Filters with a Square Matryoshka Geometry

Printed planar microstrip filters based on open Matryoshka square geometries were presented in [20, 37]. Filters with two and three rings are studied (Figure 46).

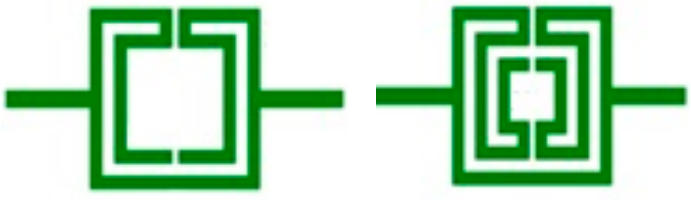

Figure 46. Open Matryoshka square geometry filters. a) With two rings. b) With three rings.

The physical characteristics of the five configurations chosen are described in Table 10. The definition of these physical characteristics is given in Figure 4. A 1.5 mm thick FR4 substrate with ε_r=4.4 and tanδ=0.02 is used. The input and output microstrip lines are 2.8 mm wide (50 Ohm characteristic impedance). W=2.0 mm and g=s=1.0 mm, are used. For the three rings configurations $L_c=L_{c1}=L_{c2}$.

 doi:10.20944/preprints202402.1017.v1

Table 10. Physical characterization of open Matryoshka geometries with two, three, and four rings.

Configuration	N	L_1 [mm]	L_2 [mm]	L_3 [mm]	L_c [mm]
Config1	2	28.0	20.0	NA	2.0
Config2			12.0		6.0
Config3			8.0		8.0
Config4	3	36.0	28.0	20.0	2.0
Config5		28.0	20.0	12.0	2.0

Photos of the fabricated prototypes are shown in Figure 47.

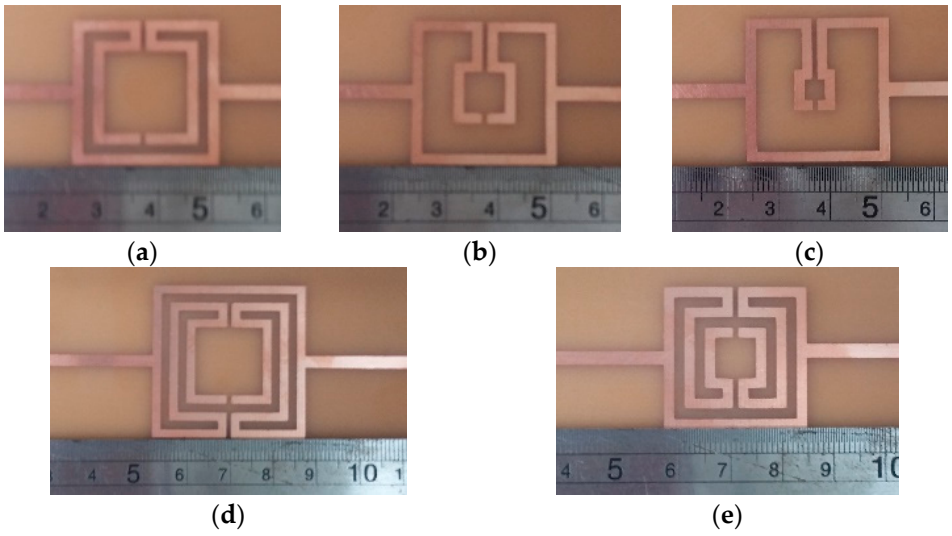

Figure 47. Photos of the prototypes of Matryoshka filters with square rings. a) Config1. b) Config2. c) Config3. d) Config4. e) Config5.

As explained in section 2, a design procedure was developed to estimate the initial dimensions of the filter that fulfill the specifications. Comparison of numerical simulation and experimental results is shown in Figure 48 (for config1, config2 and config3) and Figure 49 (for config4 and config5).

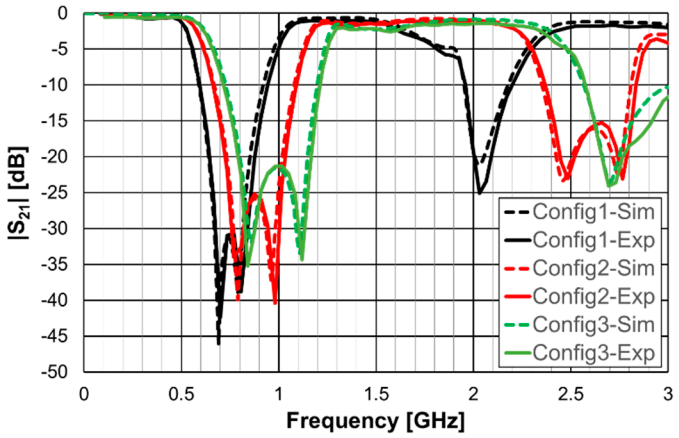

Figure 48. Comparison of $|S_{21}|$ simulation and experimental results for square Matryoshka filters config1, config2, and config3.

Figure 48 shows a very good agreement between simulation and experimental results. Table 11 summarizes the experimental characteristics of the three initial configurations.

Preprints.org (www.preprints.org) | NOT PEER-REVIEWED | Posted: 19 February 2024 doi:10.20944/preprints202402.1017.v1

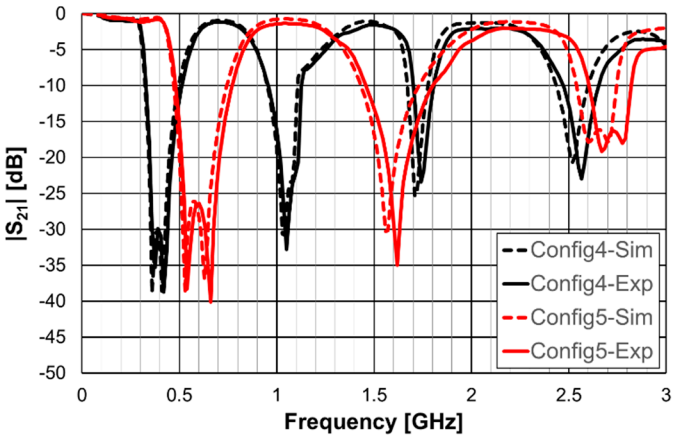

Figure 49. Comparison of $|S_{21}|$ simulation and experimental results for square Matryoshka filters config4, and config5.

In Figure 49 a very good agreement between simulation and experimental results is also obtained. Table 11 also summarizes the experimental characteristics of the two remaining configurations.

Table 11. Main experimental characteristics of the five square filter configurations.

Configuration	fr_1 [GHz]	fr_2 [GHz]	f_0 [GHz]	BW* [%]
Config1	0.700	0.805	0.769	45.4
Config2	0.770	0.980	0.876	49.0
Config3	0.840	1.120	0.964	51.4
Config4	0.375	0.420	0.421	43.8
Config5	0.540	0.660	0.626	46.4

* Defined for a -10 dB reference level.

It can be concluded that the first two resonance frequencies (f_{r1} and f_{r2}) depend on the perimeter of the rings. For the same external dimensions (L_1) the inner rings can be used to have a fine control of the stopband frequency range and of the bandwidth.

4.2. Filters with a Circular Matryoshka Geometry

Filters based on open Matryoshka circular ring configurations are studied in [26, 56]. The physical characteristics of a one ring configuration are defined in Figure 50.

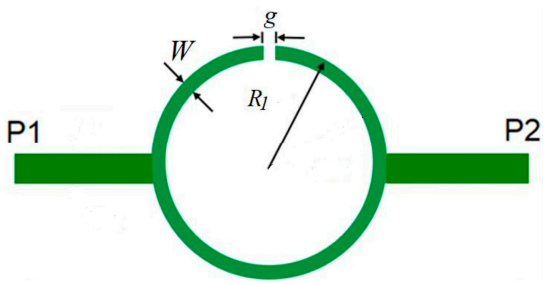

Figure 50. Stopband filter based on an open Matryoshka circular ring geometry.

Five configurations of this type of stopband filter are studied in [26] (Table 12). A 1.52 mm thick Rogers RO3003 substrate with ε_r=3.0 and tanδ=0.001 is used. The input and output microstrip lines (P1 and P2) are 3.8 mm wide (50 Ohm characteristic impedance). W=1.0 mm and g=s=1.0 mm are used.

Preprints.org (www.preprints.org) | NOT PEER-REVIEWED | Posted: 19 February 2024 doi:10.20944/preprints202402.1017.v1

Table 12. Physical characterization of open Matryoshka circular geometries with two and three rings.

Configuration	N	R1 [mm]	R2 [mm]	R3 [mm]
Config1	2	14.0	12.0	NA
Config2			10.0	
Config3			8.0	
Config4			6.0	
Config5	3		12	10.0

Photos of the fabricated prototypes are shown in Figure 51.

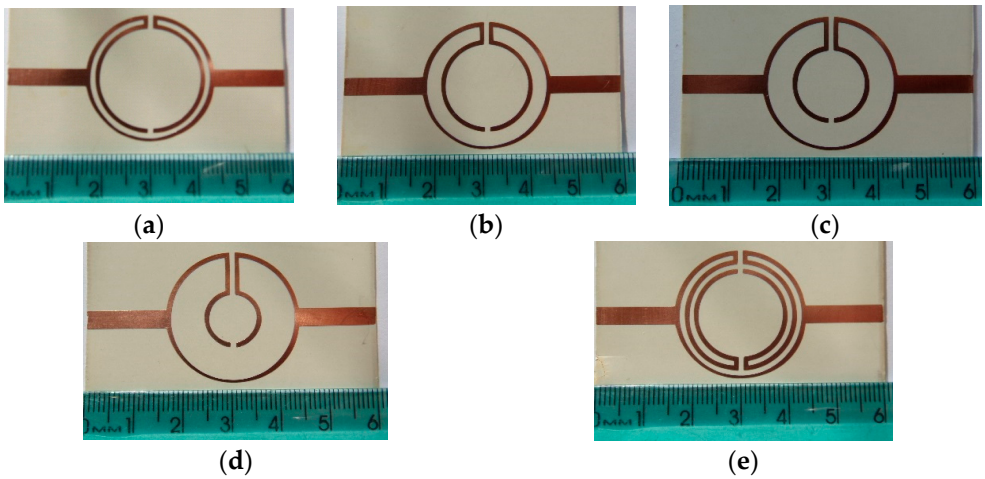

Figure 51. Photos of the prototypes of Matryoshka filters with circular rings. a) Config1. b) Config2. c) Config3. d) Config4. e) Config5.

Similarly to the square Matryoshka configurations, a design procedure was developed to estimate the initial dimensions of the filter that fulfill the specifications. Comparison of numerical simulation and experimental results is shown in Figure 52 (for config1, config2, config3, and config4) and Figure 53 (for config1 and config5).

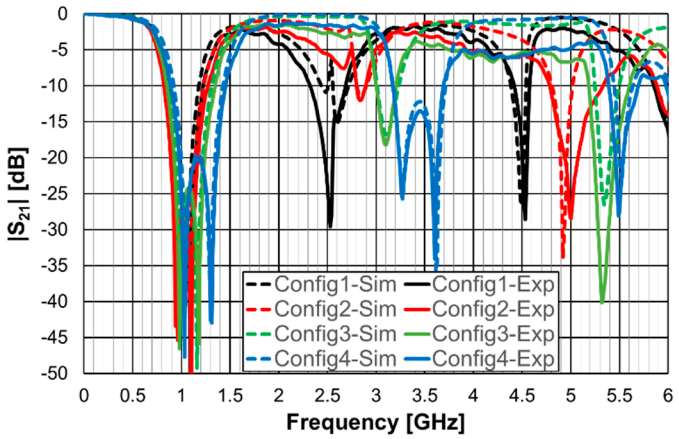

Figure 52. Comparison of $|S_{21}|$ simulation and experimental results for circular Matryoshka filters config1, config2, config3, and config4.

There is a very good agreement between the numerical simulation and the experimental results shown in Figure 52. Table 13 summarizes the experimental characteristics of the five configurations.

Preprints.org (www.preprints.org) | NOT PEER-REVIEWED | Posted: 19 February 2024 doi:10.20944/preprints202402.1017.v1

The first resonance frequency is almost independent of the second ring, but the second resonance frequency and the bandwidth increase substantially as the radius of the second ring decreases.

Table 13. Main experimental characteristics of the five circular filter configurations.

Configuration	fr_1 [GHz]	fr_2 [GHz]	f_0 [GHz]	BW* [%]
Config1	0.961	1.091	1.039	35.7
Config2	0.941	1.101	1.047	43.1
Config3	0.981	1.181	1.099	45.2
Config4	1.031	1.311	1.172	48.0
Config5	0.701	0.811	0.790	36.7

* Defined for a -10 dB reference level.

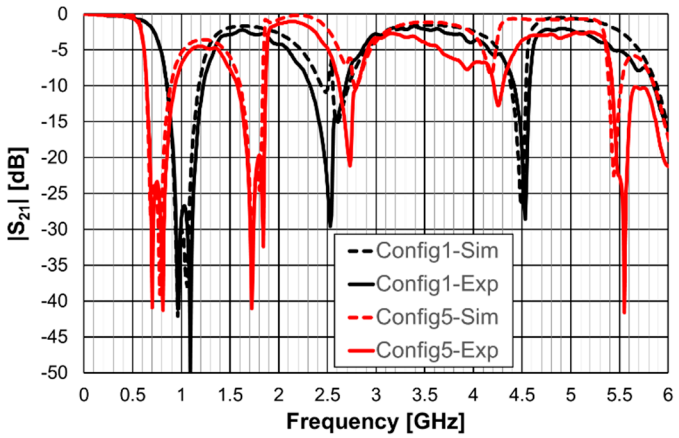

Figure 53. Comparison of $|S_{21}|$ simulation and experimental results for circular Matryoshka filters config1, and config5.

In Figure 53 a very good agreement between simulation and experimental results is also obtained. A general conclusion, in line with the analysis carried out on the filters (and also the FSSs) with square Matryoshka geometry is that, keeping the external dimension of the structure, the resonance frequency decreases (higher miniaturization) when more rings are used (higher meandering), but the bandwidth decreases.

4.3. Filters with a DGS

A DGS is formed by removing a small part from the metallic ground plane in planar printed circuit boards, most frequently in microstrip lines, as in Figure 54.

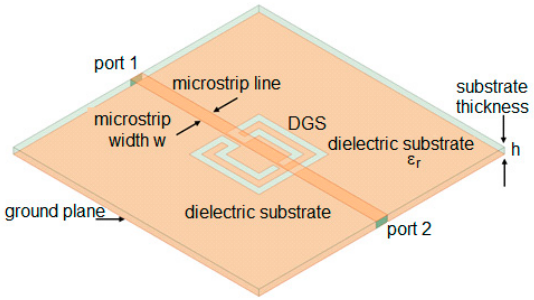

Figure 54. Example of DGS with Matryoshka geometry.

Due to ease of integration, design flexibility and compactness, DGSs have found several applications such as in planar antennas [57,58], filters [59,60], power dividers [61,62], sensors [63,64] and wireless power transfer [65,66]. A DGS based on a Matryoshka geometry, as shown in Figure 54,

Preprints.org (www.preprints.org) | NOT PEER-REVIEWED | Posted: 19 February 2024 doi:10.20944/preprints202402.1017.v1

was introduced in [30,43,67]. It is proposed in [30] a method to design this type of DGS based on simple formulas. Four configurations were designed, fabricated, and tested [30]. A 1.6 mm thick FR4 substrate (ε_r=4.4 and tanδ=0.02) is used. The corresponding dimensions are indicated in Table 14. The definition of the dimensions is provided in Figure 4.

Table 14. Physical characterization of open Matryoshka geometry DGS configurations.

Configuration	L_1 [mm]	L_2 [mm]	L_c [mm]	w [mm]	g=s [mm]
Config1	17.0	11.0	1.5	1.5	1.0
Config2	15.5	9.5			
Config3	14.0	8.0			
Config4	12.5	6.5			

Photos of the front and back sides of the prototypes are shown in Figure 55. Figure 56 provides the comparison of simulation and experimental $|S_{21}|$ results of these prototypes.

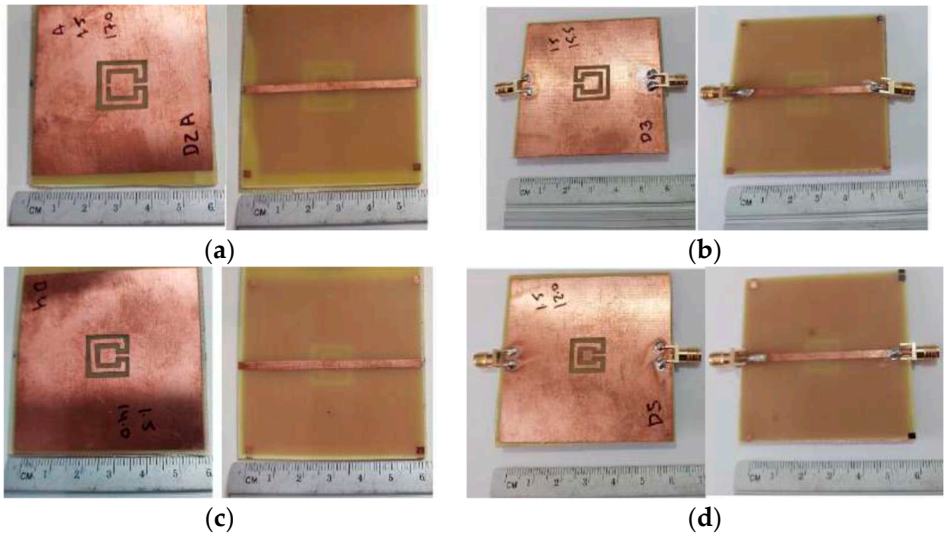

Figure 55. Photos of the microstrip line with a square Matryoshka geometry DGS configurations. a) Config1. b) Config2. c) Config3. d) Config4.

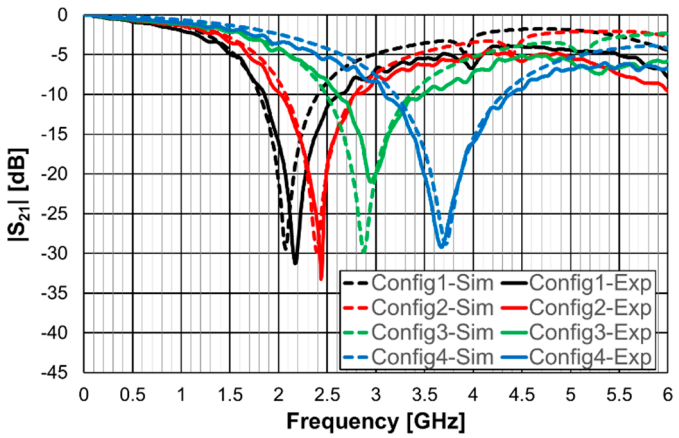

Figure 56. Comparison of $|S_{21}|$ simulation and experimental responses of a microstrip line with a square Matryoshka geometry DGS.

Good agreement is observed in Figure 56 between numerical simulation and experimental results. The tendency of the resonance frequency is the same of the metal Matryoshka configuration, that is, as the area of the structure decreases the resonance frequency increases.

Preprints.org (www.preprints.org) | NOT PEER-REVIEWED | Posted: 19 February 2024 doi:10.20944/preprints202402.1017.v1

To assess the capabilities of the Matryoshka geometry to perform as a DGS, comparison with a DGS of the common dumbbell geometry is presented in [30]. To have a fair comparison the square dumbbell geometry has the same area as the Matryoshka geometry. The simulation results for the four configurations indicated in Table 14 are presented in Figure 57.

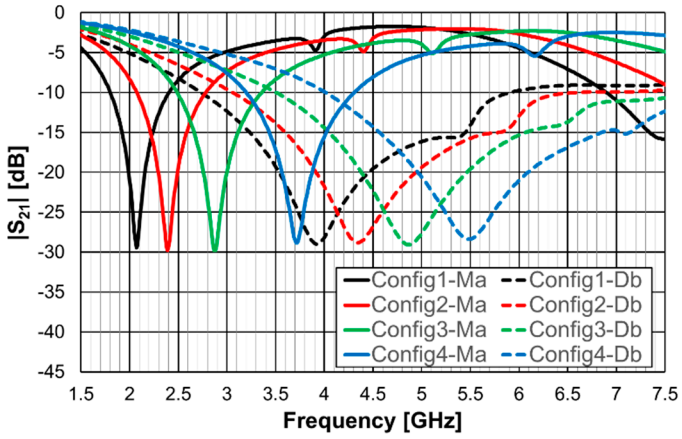

Figure 57. Comparison of $|S_{21}|$ simulation results of a microstrip line with dumbbell and Matryoshka square geometry DGS.

A summary of the results shown in Figure 57 is provided in Table 15. The resonance frequency of the Matryoshka geometry is much lower than the resonance frequency of the dumbbell geometry (larger miniaturization), but the bandwidth is much narrower.

Table 15. Physical characterization of open Matryoshka geometry DGS configurations.

Configuration	Matryoshka		Dumbbell	
	f_{r1}* [GHz]	BW [%]	f_{r1Ma}/f_{r1Db} [%]	BW_{Ma}/BW_{Db} [%]
Config1	2.07	28.8	52.8	19.0
Config2	2.39	29.3	55.1	20.0
Config3	2.88	29.8	59.1	20.0
Config4	3.72	29.6	67.9	22.3

* Defined for a -10 dB reference level.

4.4. Filters with a DGS and a Dielectric Resonator

Very recently a compact filter combining a Matryoshka geometry DGS with a high permittivity dielectric resonator was proposed [43]. The purpose is to improve the frequency response characteristics, mainly selectivity, and miniaturization. A prototype was designed, fabricated, and tested. A 1.6 mm thick FR4 substrate (ε_r=4.4 and tanδ=0.02) was used. As shown in Figure 58, a calcium cobaltite disk (ε_r=90) with diameter 10.0 mm and thickness 1.9 mm was inserted in Config3 of the previous section, below the ground plane, in contact with the DGS. A photo, with bottom view of the prototype, is shown in Figure 59. The filter transmission coefficient was simulated and measured for different positions of the dielectric disk. The corresponding results, for the disk centered on the DGS Matryoshka square geometry center, and on the DGS Matryoshka square geometry corner are shown in Figure 60. The results obtained for the filter without dielectric disk are also shown, for reference.

Preprints.org (www.preprints.org) | NOT PEER-REVIEWED | Posted: 19 February 2024 doi:10.20944/preprints202402.1017.v1

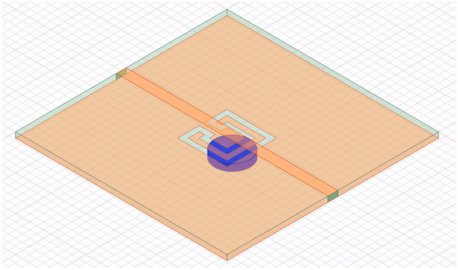

Figure 58. Filter configuration with Matryoshka square geometry DGS and dielectric resonator.

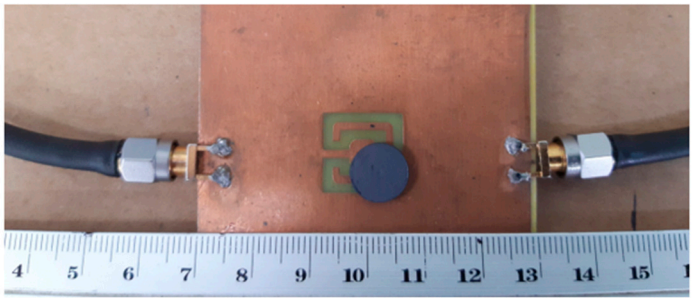

Figure 59. Photo of the prototype of the filter with Matryoshka square geometry DGS and dielectric resonator, bottom view.

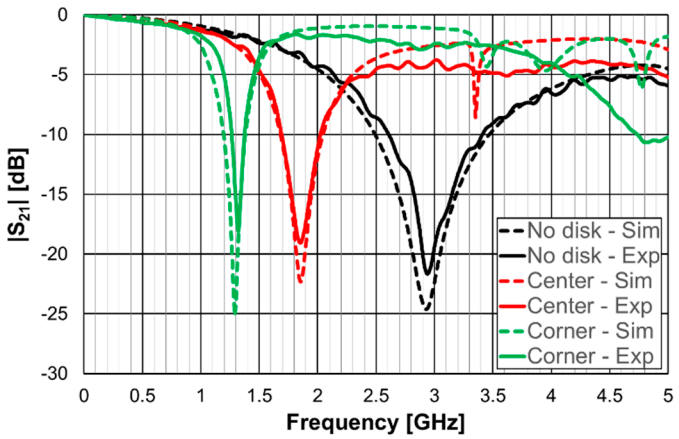

Figure 60. Comparison of $|S_{21}|$ simulation and experimental results for the square Matryoshka geometry DGS with dielectric resonator.

A very good agreement between numerical simulation and experimental results is obtained. The use of a dielectric resonator can provide further miniaturization of the structure. The experimental resonance frequency moved from 2.939 GHz (no disk) to 1.849 GHz (center) and to 1.322 GHz (corner), which corresponds to 36.8% and 55,0% reductions, respectively. Again, the price to pay is the reduction of bandwidth, which is 58.5% (center) and 86.2% (corner), respectively. The position of the dielectric disk can be used to fine tune the central frequency of the filter's response.

5. Examples of Application as Antenna

Due to their inherent multiresonant characteristics Matryoshka geometries are suitable for multiband and/or wideband antenna configurations [25,28]. Moreover, because of the meandering of the nested rings they have also been used to provide antenna miniaturization [25,28]. These features can be advantageously combined with printed antennas in general and microstrip patch antennas in particular [25,28]. Microstrip is one of the most successful antenna technologies. Such success stems

 doi:10.20944/preprints202402.1017.v1

from well-known advantageous and unique properties, such as a low profile, light weight, planar structure (but also conformal to non-planar geometries), mechanical strength, easy and low-cost fabrication, easy integration of passive and active components, easy combination to form arrays, and outstanding versatility in terms of electromagnetic characteristics (resonance frequency, input impedance, radiation pattern, gain, polarization). Microstrip patch antennas can be used in a very wide frequency range, extending roughly from about 1 GHz to 100 GHz [68]. So far, the Matryoshka geometries have been used in microstrip patch antennas to modify the ground plane and implement it as a DGS [25,28]. DGSs have been used in microstrip antenna implementations to provide multiband and/or wideband behavior, improve gain and cross-polarization, and suppress higher order modes and mutual coupling (in arrays) [69-73]. Many different shapes of the DGS slots have been used, ranging from canonical geometries (rectangular, triangular, circular), to non-canonical (H-shaped, dog bone-shaped) [74]. Recently, such variety was enhanced with the Matryoshka geometry [25,28].

In [25] a comparison of the performance of a microstrip patch antenna with a DGS ground plane with circular SRRs [75] and Matryoshka geometries is presented. The emphasis is on the open Matryoshka configuration. In [28] a detailed comparative analysis of the performance of open and closed Matryoshka DGS geometries is carried out. In all the cases, a cheap FR4 substrate with relative electric permittivity 4.4, thickness 1.6 mm and loss tangent 0.02 was used.

5.1. Reference Microstrip Patches

In [25], as an application example, the dimensions of a rectangular patch were chosen to provide the first resonance at 2.5 GHz. The initial dimensions obtained with the transmission line method [76] were optimized using ANSYS Designer software tool [77]. A patch width (W) 37.0 mm, length (L) 27.8 mm and a square ground plane with a 53.0 mm side were chosen. The patch is fed with a 2.8 mm wide microstrip transmission line (50 Ohm characteristic impedance) and inset 1 mm wide and 8 mm long. The corresponding simulated input reflection coefficient is shown in Figure 61, for reference.

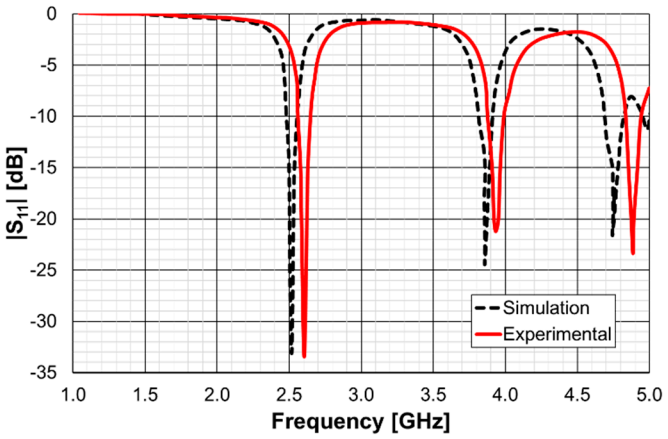

Figure 61. Simulation and experimental input reflection coefficient of the simple rectangular patch.

The first resonance (2.52 GHz), the second resonance (3.86 GHz) and the third resonance (4.74 GHz) are well matched to the 50 Ohm feed microstrip transmission line. To validate the design procedure used, a protype of the microstrip patch antenna was fabricated using a conventional photolithography technique. The amplitude of the experimental input reflection coefficient ($|S_{11}|$), also shown in Figure 61, was measured with an Agilent E5071C vector network analyzer. Taken into account that the FR4 substrate used is low cost, and its characteristics are only generically known, there is a good agreement between numerical simulations and experimental results. For the frequency of interest (first resonance) the difference in the frequency is only 3.4% (88 MHz) and the $|S_{11}|$ level is almost the same (-33 dB). This antenna presents the usual almost hemispherical broadside radiation pattern [76] with a gain of 6.18 dBi at 2.52 GHz.

Preprints.org (www.preprints.org) | NOT PEER-REVIEWED | Posted: 19 February 2024 doi:10.20944/preprints202402.1017.v1

Another microstrip patch was designed so that using a DGS ground plane the same first resonance (2.5 GHz) of the simple patch, described above, could be obtained [25]. In this case the patch was designed to have alone the first resonance frequency at 3.5 GHz. The patch and ground plane sizes were 28.0 mm (W), 20.0 mm (L) and 38.0 mm, 45.0 mm, respectively. The corresponding simulation and experimental input reflection coefficient is shown in Figure 62.

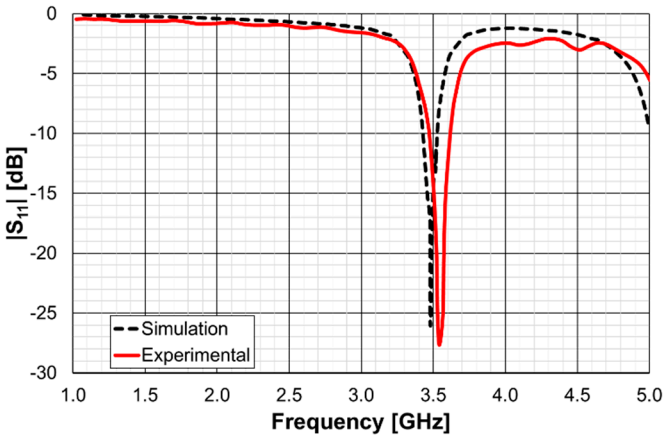

Figure 62. Simulation and experimental amplitude of the input reflection coefficient of the simple rectangular patch.

The difference in the simulation and experimental resonance frequencies is only 2.0% (69 MHz) and the $|S_{11}|$ level is below -26 dB, for both curves.

5.2. DGS Uni-Cell

From initial exploratory simulations [25] it is concluded that the patch with a DGS would present the first resonance frequency at 2.5 GHz when the DGS unit-cell alone had the first resonance at about 2.6 GHz. Therefore, both the complementary open Matryoshka and circular SRR configurations were designed to provide such 2.6 GHz first resonance frequency. To take into account the intrinsic characteristics of the unit-cells their analysis was done considering an infinite FSS with 20x20 mm^2. The two configurations are shown in Figure 63. Ansys HFSS [77] was used for the simulations.

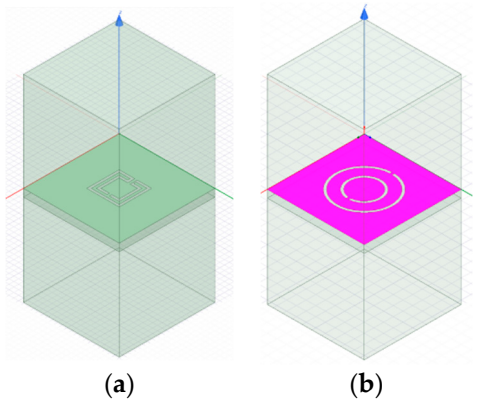

Figure 63. FSS unit-cells. a) Complementary open Matryoshka geometry. b) Complementary circular SRR geometry.

The complementary open square Matryoshka configuration has dimensions L_1=6.8 mm and L_2=4.8 mm. For the circular complementary SRR r_1=5.4 mm and r_2=3.5 mm was used. In both cases, the trace and slot widths are 0.50 mm and 0.25 mm, respectively. The simulated $|S_{21}|$ results are shown in Figure 64.

 doi:10.20944/preprints202402.1017.v1

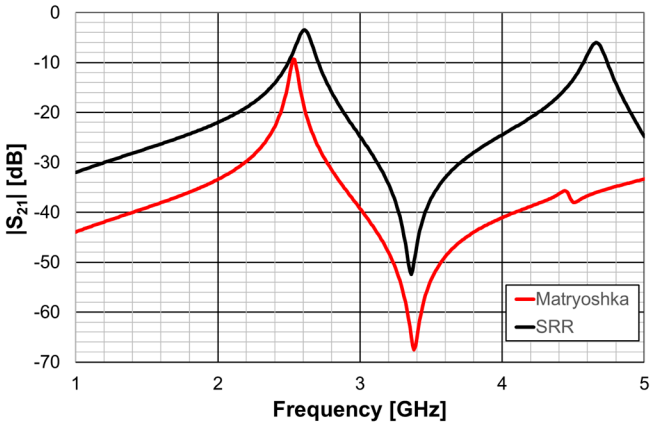

Figure 64. Simulation $|S_{21}|$ results of the open square Matryoshka and SRR FSS configurations.

It can be concluded that, as required, both unit-cells provide the first resonance frequency at about 2.6 GHz

5.3. Patch with DGS

The patch's ground plane was changed by the introduction of a DGS with an open square Matryoshka and a circular SRR [25], as shown in Figure 65.

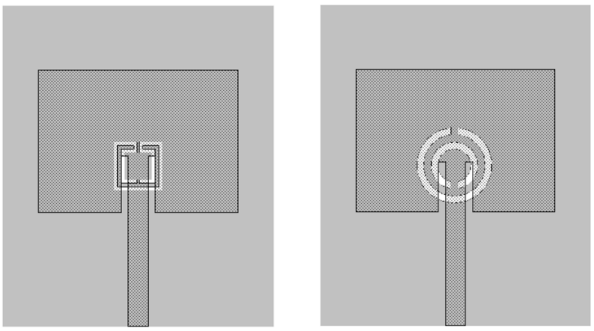

Figure 65. Microstrip patch with DGS. a) Square Matryoshka geometry. b) Circular SRR geometry.

The simulation and experimental results for the amplitude of the input reflection coefficient, for both DGS unit-cell geometries, are shown in Figure 66.

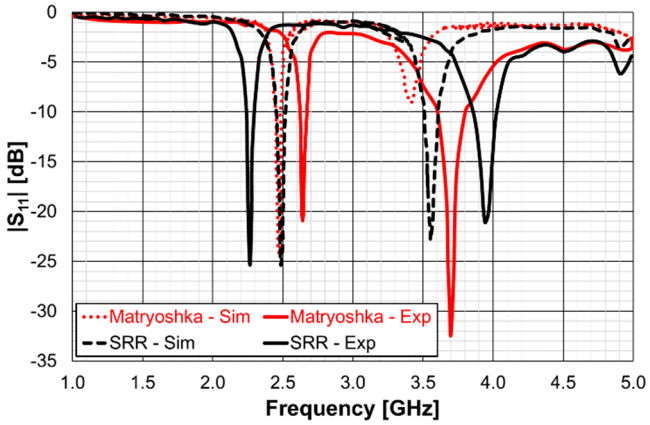

Figure 66. Simulation and experimental $|S_{11}|$ results of the patch with DGS ground plane.

 doi:10.20944/preprints202402.1017.v1

There are some differences between simulation and experimental results. For the first resonance frequency the experimental result for the SRR geometry is 8.8% (218 MHz) below the simulation one whereas for the Matryoshka geometry the experimental result is 6.7% (165 MHz) above the simulation. These differences are mainly caused by the inaccuracy of the fabrication process mostly related with the narrow (0.25 mm) slots. However, these unwanted differences do not jeopardize the envisage proof of concept, that is, both the DGS configurations provide a remarkable miniaturization of about 46% (in the area of the microstrip patch).

The farfield radiation patterns of the patch with the two DGS configurations are shown in Figures 67–69.

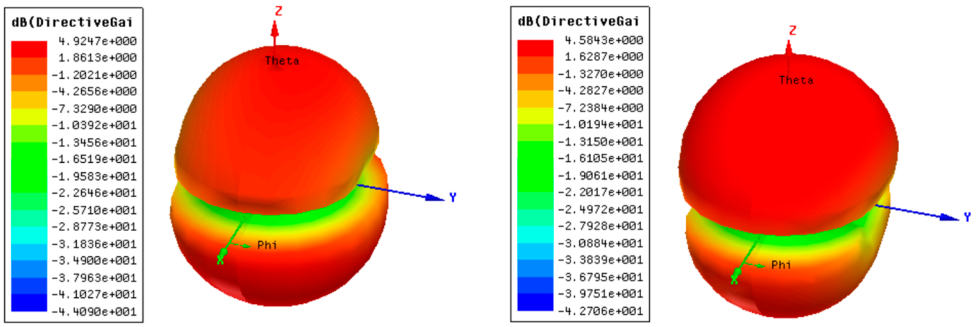

(**a**) (**b**)

Figure 67. Simulation 3D radiation pattern (gain scale) of the patch with DGS at the first resonance frequency. a) Matryoshka geometry. b) SRR geometry.

When compared with the radiation pattern of the common patch the main difference is the high radiation level below the ground plane. In contrast with the typical hemispherical type of radiation pattern observed for the common microstrip patch [76] a bi-hemispherical type of radiation pattern is caused by the DGS. This was expected, first due to the introduction of slots in the ground plane and second because the slots are near resonance and therefore with enhanced radiation. This type of radiation pattern may be interesting for application where a more uniform spatial radiation power distribution is required. For the DGS with Matryoshka geometry the maximum gain (4.9 dBi) is obtained in the back hemisphere ($\theta \approx 180^{o}$). For the DGS with SRR geometry the direction of maximum radiation is kept on the front hemisphere ($\theta \approx 0$), with 4.6 dBi gain, but the front-to-back (FBR) ratio is low (2.8 dB). The drop of about 1.4 dB in the gain is related to the more uniform distribution of radiated power in space.

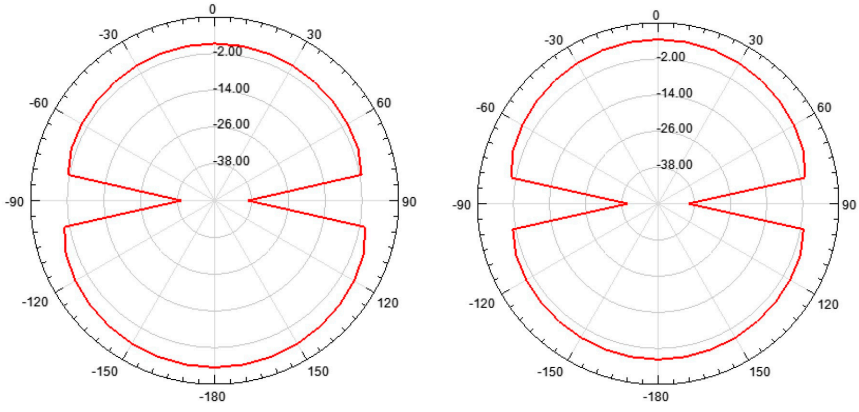

(**a**) (**b**)

Figure 68. Simulation H-plane radiation pattern (gain scale) of the patch with DGS at the first resonance frequency. a) Matryoshka geometry. b) SRR geometry.

Preprints.org (www.preprints.org) | NOT PEER-REVIEWED | Posted: 19 February 2024 doi:10.20944/preprints202402.1017.v1

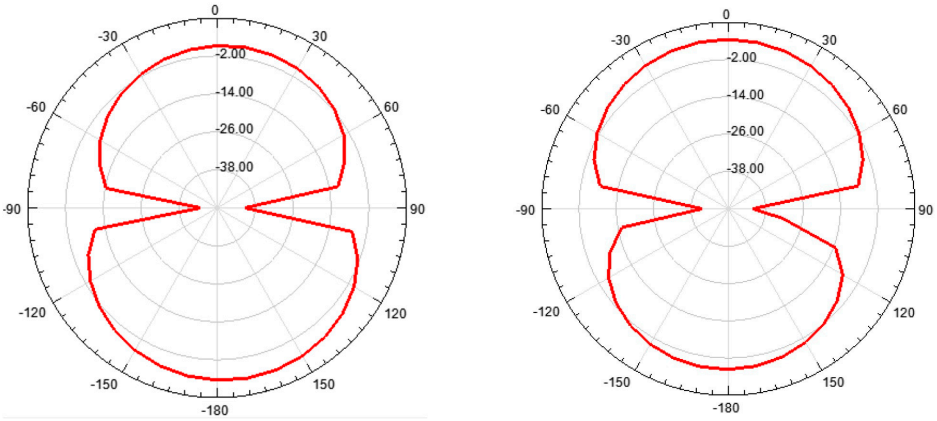

Figure 69. Simulation E-plane radiation pattern (gain scale) of the patch with DGS at the first resonance frequency. a) Matryoshka geometry. b) SRR geometry.

The main radiation characteristics, obtained by simulation, are summarized in Table 16.

Table 16. Summary of simulated radiation pattern results at the first resonance frequency.

Parameter		Matryoshka	SRR
Direction of maximum radiation (θ) [Degree]		≈180	≈0
Maximum gain [dBi]		4.9	4.6
Half-power beamwidth [Degree]	H-Plane	140	137
	E-Plane	87	86
FBR [dB]		-3.2	2.8

A fair comparison of the miniaturization capability of the two DGS geometries under analysis (open Matryoshka and circular SRR) must consider unit-cells with the same dimension. The first resonance frequency of the microstrip patch with DGS ground plane, as a function of the maximal dimension (side of the square open Matryoshka geometry and diameter of the circular SRR), is shown in Figure 70.

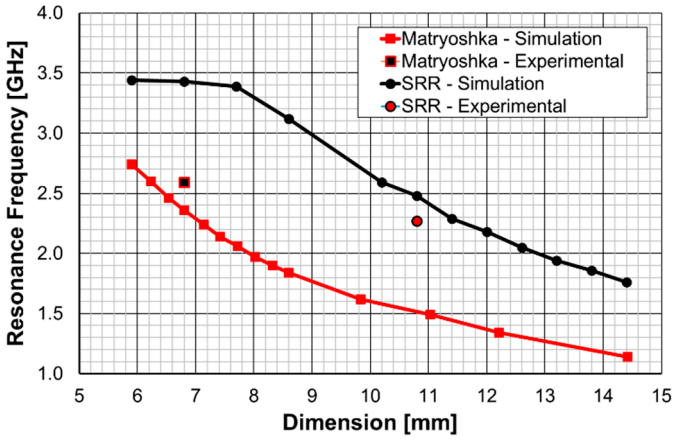

Figure 70. Simulation results for the first resonance frequency of the DGS unit-cell.

As it can be observed, the open Matryoshka geometry provides much lower simulation results for the frequency of the first resonance. Moreover, the experimental results obtained for the two fabricated prototypes, have a reasonable agreement with the simulations (difference less than 9%). The average difference, for the resonance frequencies associated with each DGS geometry, is almost 1 GHz (0.94 GHz) which corresponds to 35.4%. This proves that the proposed open Matryoshka geometry has a much stronger miniaturization capability than the conventional circular SRR.

 doi:10.20944/preprints202402.1017.v1

In a very recent work [28] a detailed analysis of the effects of a DGS with a Matryoshka unit-cell in the ground plane of a microstrip patch is carried out. A complete sensitivity analysis of the influence of the geometric parameters of the unit-cells in the antenna performance was conducted. The main conclusions obtained in [25] are confirmed and are supported by an extensive and systematic analysis, with simulations and experimental validation. The emphasis is on the comparison of the miniaturization capabilities of the open and the closed complementary Matryoshka geometries. As an example, some results obtained for an optimized configuration are reproduced below.

The two configurations of the microstrip patch with a DGS ground plane, that is, with open and closed Matryoshka cells, are shown in Figure 71.

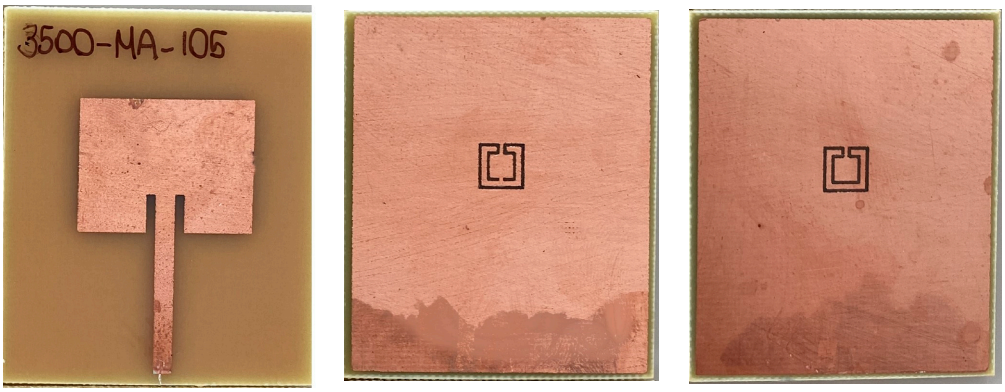

(**a**) (**b**) (**c**)

Figure 71. Microstrip patch antenna prototypes with DGS complementary Matryoshka cells. a) Patch side. b) Ground-plane side with open Matryoshka geometry cell. b) Ground-plane side with closed Matryoshka geometry cell.

The $|S_{21}|$ of a 50 Ohm microstrip line with a DGS with open and closed Matryoshka square geometries (Figure 72) (L_1=7.5 mm, L_2=4.5 mm, w=0.5 mm and s=g=0.5 mm), as a function of frequency is shown in Figure 73. The measurement setups used are shown in Figure 74.

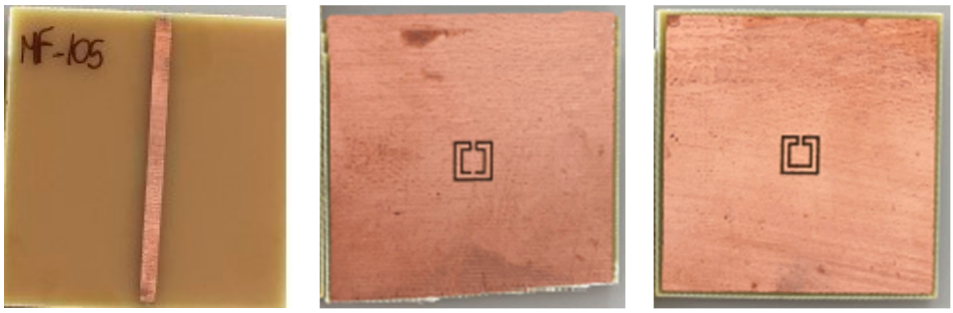

(**a**) (**b**) (**c**)

Figure 72. Microstrip line prototypes with DGS complementary Matryoshka cells. a) Microstrip line side. b) Ground-plane side with open Matryoshka geometry cell. b) Ground-plane side with closed Matryoshka geometry cell.

 doi:10.20944/preprints202402.1017.v1

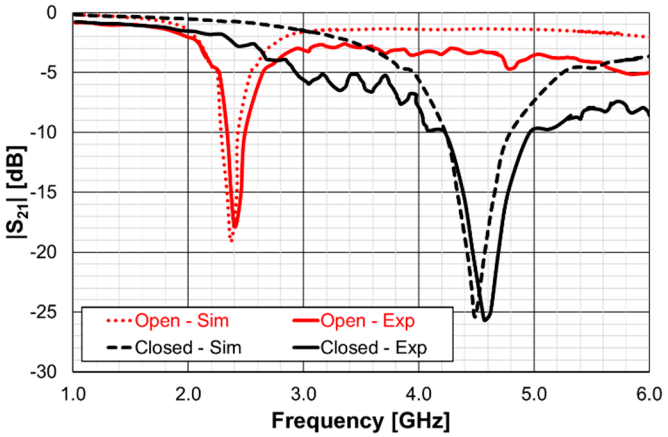

Figure 73. $|S_{21}|$ results for the microstrip line with a DGS with open and closed square Matryoshka cells.

Figure 74. Setups used for the experimental characterization of the microstrip patch and microstrip line with a DGS with open and closed square Matryoshka cells.

There is a good agreement between simulation and experimental $|S_{21}|$ results. Although the open and closed Matryoshka unit-cell have the same dimensions the first resonance of the open structure (2.40 GHz) is 47.4% below the first resonance of the closed structure (4.57 GHz). However, the closed structure has a much wider -10 dB bandwidth (560 MHz compared with 150 MHz). As shown in Figure 75, this reduction leads also to a reduction of the first resonance frequency of the patch with the open Matryoshka DGS.

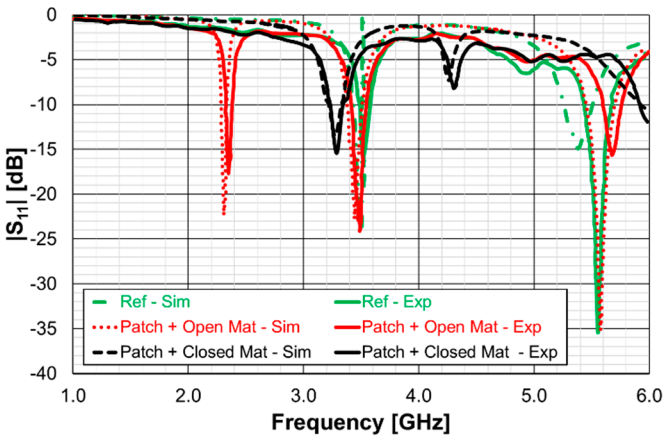

Figure 75. Amplitude of the input reflection coefficient of the patch without and with DGS ground plane.

 doi:10.20944/preprints202402.1017.v1

The input reflection coefficient of the common patch (without DGS) is also shown for reference in Figure 75. In this case the microstrip patch antenna with open Matryoshka DGS presents the first resonance frequency at 2.35 GHz which is 28.5% below the first resonance of the microstrip patch antenna with closed Matryoshka DGS (3.29 GHz) and 33.2% below the first resonance of the microstrip patch antenna with solid ground plane (3.52 GHz).

The surface current distribution, shown in Figure 76, provides physical insight into the antenna's radiation mechanisms. The current distribution on the common patch (without DGS) is also shown, for reference.

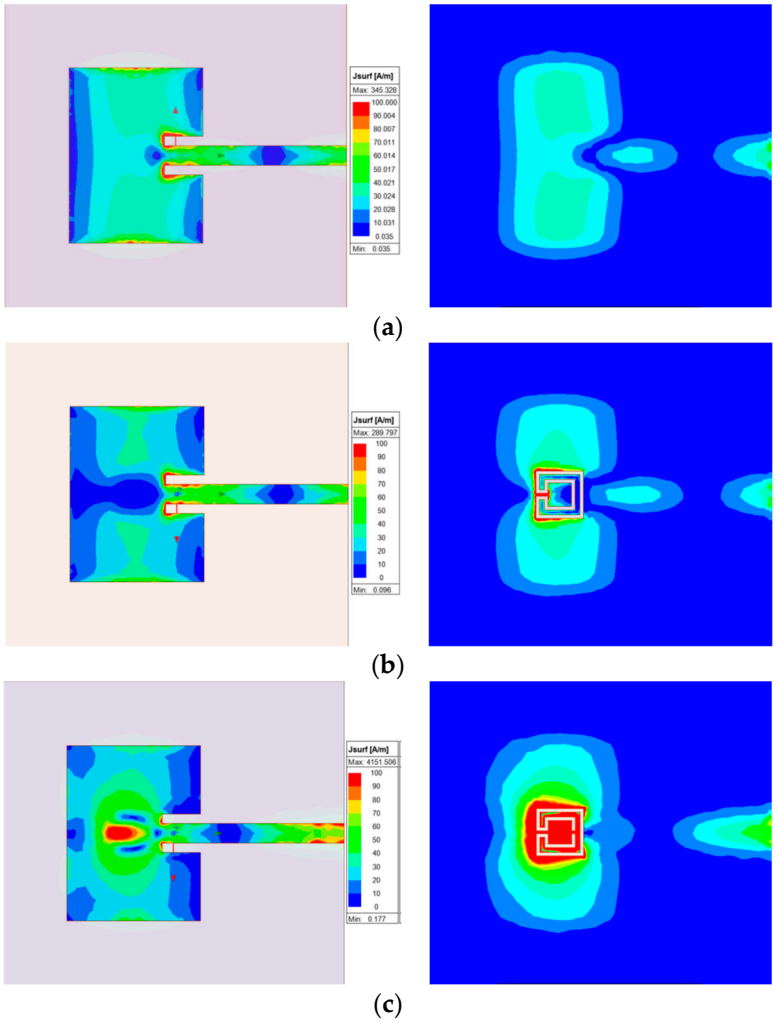

Figure 76. Current distribution on the microstrip patch and ground plane at the first resonance frequency. a) Common patch. b) Patch with closed Matryoshka DGS. c) Patch with open Matryoshka DGS.

As expected, the presence of the DGS changes enormously the current distribution not only on the ground plane but also on the patch. This change is more effective for the open Matryoshka geometry. The almost constant current distribution along the common patch width is strongly perturbed by the DGS.

The 3D radiation patterns of the patch with a DGS, with closed and open Matryoshka geometries, are shown in Figure 77. Again, the radiation pattern of the common patch (without DGS) is also shown, for reference.

The maximum gain for the common patch, the patch with closed Matryoshka DGS and the patch with open Matryoshka DGS are 4.24 dBi, 3.55 dBi and 2.40 dBi, respectively. Naturally the increase of the back radiation caused by the DGS, implies a decrease of the maximum gain, especially for the open Matryoshka DGS.

 doi:10.20944/preprints202402.1017.v1

A summary of the main results obtained for the patch antenna without DGS and with DGS with open and closed Matryoshka geometries is presented in Table 17.

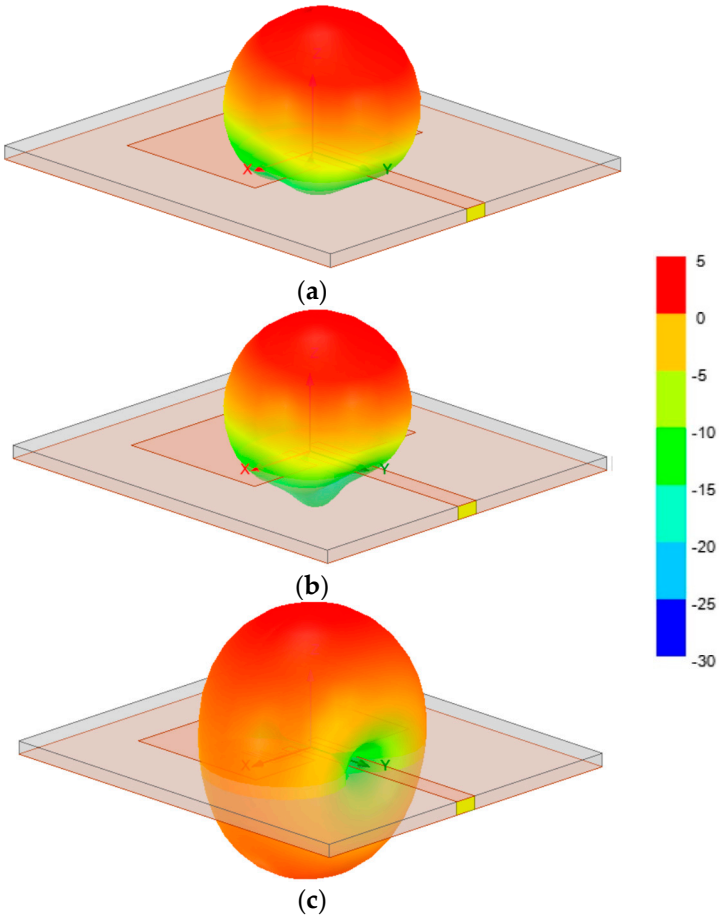

Figure 77. 3D radiation pattern (gain scale) of the microstrip patch at the first resonance frequency. a) Common patch. b) Patch with closed Matryoshka DGS. c) Patch with open Matryoshka DGS.

Table 17. Summary of the main patch antenna characteristics.

Parameter		Without DGS	With open Matryoshka	With closed Matryoshka
First resonance frequency [GHz]		3.52	2.35	3.29
-10 dB bandwidth	[MHz]	92	53	108
	[%]	2.6	2.3	3.3
Gain [dBi]		4.24	2.40	3.55

It can be concluded that both Matryoshka DGS geometries provide miniaturization, but the open structure is much more effective. However, both Matryoshka DGS geometries cause a decrease in the gain, being more pronounced for the open structure. The open structure also provides a narrower impedance bandwidth.

6. Examples of Application as Sensor

If a material under test (MUT) is incorporated in a filter and the filter changes its frequency response according to the characteristics of the MUT, this filter can be used as a sensor [78]. Based on this idea, 3 practical sensors have been proposed.

 doi:10.20944/preprints202402.1017.v1

6.1. Alcohol Concentration Sensor

A new and simple sensor, based on a microstrip filter with an open Matryoshka configuration was proposed in [34]. The proposed sensor was designed, fabricated, and successfully applied to detect the alcohol content of a liquid. Photos of the prototype and of the measurement setup are shown in Figure 78. A small acrylic container with internal dimensions 43.7x43.7x30.0 mm^3 (57.29 ml capacity) and 3.0 mm and 1.0 mm thick side and bottom walls, was placed over the filter, centered on the Matryoshka geometry.

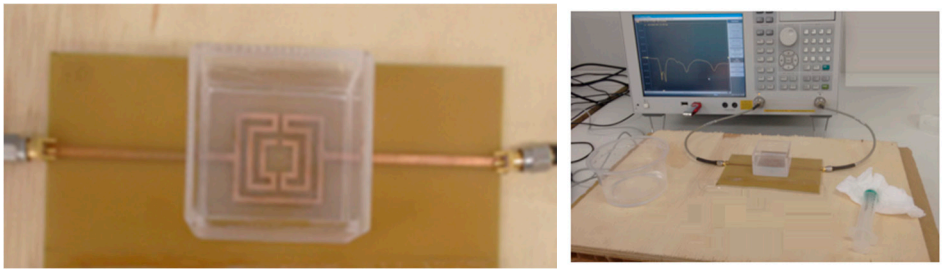

Figure 78. Prototype of the alcohol concentration sensor and of the measurement setup.

The experimental results obtained for the first resonance frequency, as a function of the alcohol concentration, for three different volumes of liquid, is shown in Figure 79.

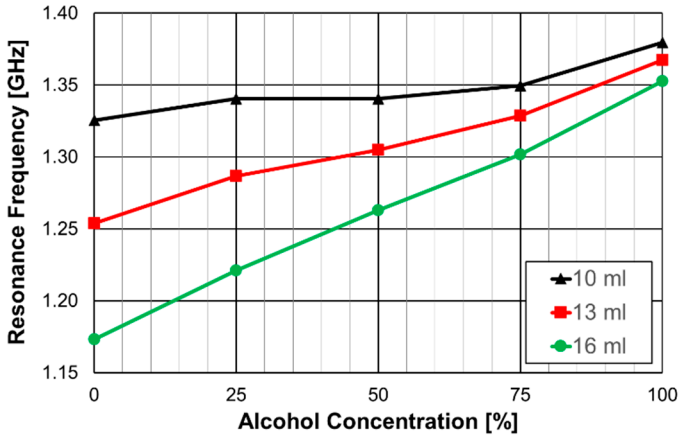

Figure 79. Resonance frequency for different alcohol concentration and volume.

For a 16 ml volume of the MUT (about 8.4 mm of liquid in the container) the response is almost linear. It is clear that the larger the MUT volume the better the sensitivity (slope of the curve) is. Based on the design procedure described in section 4.1, other prototypes can be fabricated to develop sensors to be used on other frequency bands. Moreover, other liquids can be characterized, based on calibration curves previously validated.

6.2. Sucrose Level and Water Content Sensors

In [79] a sensor based on a microstrip filter with a Matryoshka geometry DGS is used to obtain the sucrose level of an aqueous solution. Based on the analysis and design procedure described in section 4.3 the prototype, shown in Figure 80, was developed. It is based on the configuration 1 described in Table 14.

 doi:10.20944/preprints202402.1017.v1

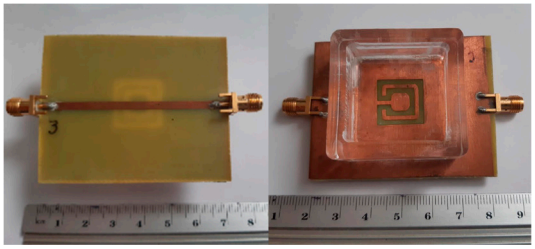

Figure 80. Prototype of the Matryoshka geometry DGS sensor. a) Bottom view. b) Top view with container.

A small acrylic container with internal dimensions 30x30x15 mm^3 (13.5 ml capacity) was placed over the filter, centered on the Matryoshka geometry. The filter is used upside down, that is, with the DGS on the top side.

The calibration curve obtained for the determination of the sucrose level in an aqueous solution is shown in Figure 81.

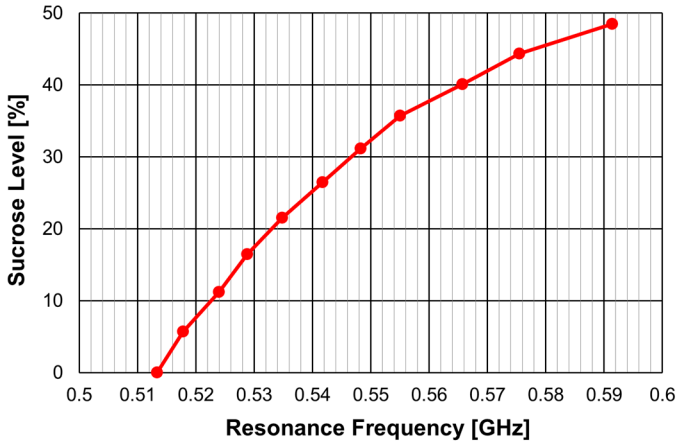

Figure 81. Calibration curve for sucrose level content sensor.

A similar sensor is proposed in [41] to determine the distilled water content in a solution of isopropyl alcohol and distilled water. It is based on configuration 2 described in Table 14. The corresponding calibration curve is reproduced in Figure 82.

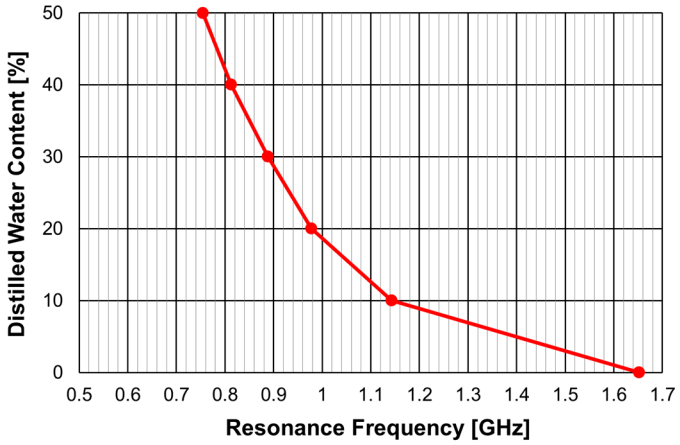

Figure 82. Calibration curve for distilled water content sensor.

 doi:10.20944/preprints202402.1017.v1

6.3. Soil Moisture Sensor

In [31,44] a new soil moisture sensor based on a filter with a Matryoshka geometry DGS is described. The filter configuration is represented in Figure 83.

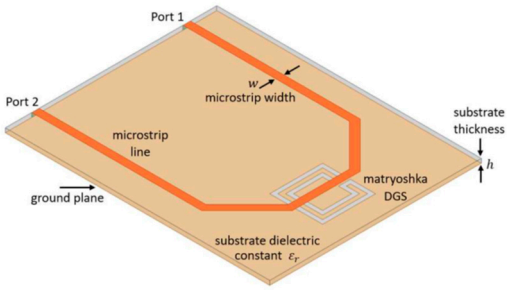

Figure 83. Structure of the filter configuration used as soil moisture sensor.

A closed Matryoshka geometry DGS with L_1=20.0 mm, L_2=14.0 mm, w=2.0 mm and g=1.0 mm is used. Photos of the prototype and of the measurement setup are shown in Figure 84.

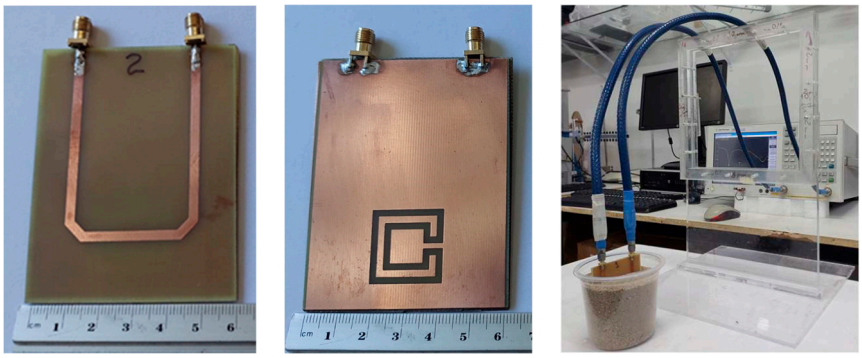

(**a**) (**b**) (**c**)

Figure 84. Photos of the experimental validation process. a) Microstrip line side view. b) DGS side view. c) Measurement setup.

Two types of soil were measured: a sandy soil usually used in civil construction, with about 98% sand, and a garden soil rich in organic substances. The corresponding experimental results are shown in Figure 85. So far, the resonance frequency has been used but in this case the frequency points where $|S_{21}|$ reaches the -6 dB level is used because it is more stable [31,44].

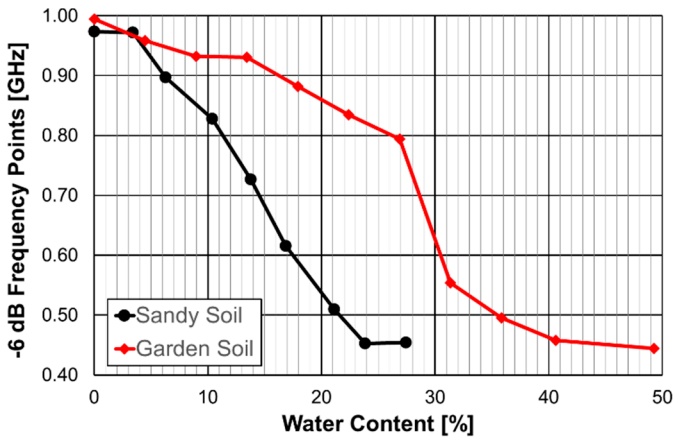

Figure 85. Experimental resonance frequency results for sandy and garden soils.

 doi:10.20944/preprints202402.1017.v1

As the water content increases the sandy soil absorbs less water and the sample saturates more quickly, starting from approximately 24%. On the other hand, garden soil absorbs more water, and the saturation point occurs at about 40%.

7. Conclusions and Perspectives of Future Developments

This paper reviews the research activities developed on the topic of printed planar resonator structures nested inside each other, called Matryoshka geometries. These research activities started about 10 years ago and most of the work has been done at the Group of Telecommunications and Applied Electromagnetism (GTEMA) from the Instituto Federal da Paraíba, in João Pessoa, Brazil. Although it is still a recent topic, much and varied work has been done to describe the different types of structures, discover and explain their properties, get physical insight on the working principles, and explore potential applications.

The main characteristics of Matryoshka geometries stem from their meandered nature and the fact that the area occupied is defined by the external ring where the other interconnected rings are nested inside. These characteristics render them strong miniaturization capability and selective multi-resonances that are highly attractive to be used in many microwave devices. The initial application as FSS was quickly extended to other applications, such as, filters, antennas, and different types of sensors.

The Matryoshka geometry is described initially, and the closed and open configuration are introduced. The physical parameters that describe the geometry are defined. The main common characteristics are analyzed, and the working principles studied to provide physical insight on their behavior.

The initial application of Matryoshka geometries, as FSS unit-cells, is fully examined. Closed and open configurations are analyzed in detail and comparison with simple rings is provided. The sensitivity of the transmission coefficient to each of the physical parameters is evaluated. To overcome the polarization dependence of simple FSS configurations, polarization independent Matryoshka geometry configurations are introduced and analyzed. Combination of an FSS with crossed dipole is proposed to enhance the multi-frequency response. Complimentary configurations, where the Matryoshka geometries are implemented with slots, are also analyzed. FSS unit-cells that use PIN diodes to provide reconfigurability are proposed and studied. It is effectively verified that in all the configurations studied the Matryoshka geometry based configurations exhibit the expected multi-resonance behavior and a remarkable miniaturization is provided.

Microstrip filters that used both square and circular rings with the open Matryoshka geometry are thoroughly examined. Configurations with different dimensions and number of rings are studied. The use of open Matryoshka geometries, to implement DGS (in the ground plane) in microstrip filters is also proposed and analyzed. A combination of an open Matryoshka DGS configuration with a dielectric disk resonator is proposed to further enhance the miniaturization capability.

The use of DGS configurations with Matryoshka geometry in the ground plane of microstrip patch antennas is proposed and examined in detail. It is concluded that there is a remarkable miniaturization capability, but a decrease of gain and impedance bandwidth is observed inevitably.

Some applications of the devices based on configurations with Matryoshka geometries have already been envisaged and reported. Microstrip filters with open Matryoshka geometry are used to determine the alcohol concentration present in a liquid solution. The quality of the estimation increases as the volume of the sample increases. A microstrip filter with closed Matryoshka geometry DGS is used in a sensor conceived to obtain the sucrose content level and the distilled water content level of aqueous solutions. The corresponding calibration curves are proposed. Another microstrip filter with close Matryoshka geometry is used to obtain the percentage of moisture in soil samples. These applications of Matryoshka based geometry configurations in sensors are very promising because they are simple, low-cost, and potentially accurate.

Although many configurations based on Matryoshka geometries have been proposed and some potential applications of them as FSSs, filters, antennas and sensors have been explored, it is clear that much more remains to be investigated. This is natural since it is just a ten year old activity, and,

therefore, many possibilities can be envisaged. Possible topics of future work are: better compression of higher order resonances, the effect of the strip (stopband), or slot (passband) width and, in the case of open rings, the positioning of the gap. Some work is already being carried out, including passband filters in multilayer structures, for which the first results should be published soon. Similarly, double-sided FSS are being implemented. Optimized Matryoshka geometry based DGS sensors for a specific application is also something that can be developed.

We would also like to highlight that the applications developed so far are conceptual and limited to manufacturing processes available on a laboratory scale. Much more can be done from the concepts presented.

Concluding, we highlight that the investigation of the applications of Matryoshka geometries is an open field, whose results obtained so far encourage other groups to get involved in this research effort.

Author Contributions: Conceptualization, AN, JS and JC; methodology, AN, JS and JC; software, AN, JS and JC; validation, AN, JS, and JC; formal analysis, AN, JS, JC and CP; investigation, AN, JS and JC; resources, AN, JS and JC; data curation, AN, JS and JC; writing—original draft preparation, AN, JS, JC and CP; writing—review and editing, AN, JS, JC and CP; visualization, AN, JS, JC and CP; supervision, AN, JS and JC; project administration, AN, JS and JC; funding acquisition, AN, JS, JC and CP. All authors have read and agreed to the published version of the manuscript.

Funding: This work was funded by Instituto Superior Técnico (IST), Instituto de Telecomunicações (IT) and Fundação para a Ciência e a Tecnologia (FCT) under grant UIDB/50008/2020. This work was supported in part by the Brazilian National Council for Scientific and Technological Development (CNPq)-Brazil, under project 309412/2021-8, in part by the Federal Institute of Paraíba (IFPB), under projects 21/2022 and 22/2022, and Electrical Engineering Graduation Program, PPGEE-IFPB, and in part by the Project FAPESQ/CAPES Nº 18/2020.

Acknowledgments: The authors acknowledge the dedicated work done by the MSc students listed in the references.

Conflicts of Interest: The authors declare no conflict of interest.

References

1. Moon, S.; Khanna, S. K.; Chappell, W. J. Multilayer Silicon RF System-in-Package Technique Using Magnetically Aligned Anisotropic Conductive Adhesive. In Proceedings of IEEE MTT-S International Microwave Symposium, Boston MA, USA, 7-12 June 2009. https://doi.org/10.1109/MWSYM.2009.5165817
2. Hu, F.; Hao, Q.; Lukowiak, M.; Sun, Q.; Wilhelm, K.; Radziszowski, S.; Wu, Y. Trustworthy Data Collection from Implantable Medical Devices Via High-Speed Security Implementation Based on IEEE 1363. *IEEE Transactions on Information Technology in Biomedicine* **2010**, *14*, 1397-1404. https://doi.org/10.1109/TITB.2010.2049204
3. Ahmad, R.; Kuppusamy, P.; Potter, L. C. Nested Uniform Sampling for Multiresolution 3-D Tomography. In Proceedings of IEEE International Conference on Acoustics, Speech and Signal Processing, Dallas, TX, USA, 14-19 March 2010. https://doi.org/10.1109/ICASSP.2010.5495713
4. Ghali, C.; Hamady F.; Elhajj, I. H.; Kayssi, A. Matryoshka: Tunneled Packets Breaking the Rules. In Proceedings of International Conference on High Performance Computer & Simulation, Istanbul, Turkey, 4-8 July 2011. https://doi.org/10.1109/HPCSim.2011.5999864
5. Raj, N. N.; Brijitta J.; Ramachandran D.; Rabel A. M.; Jayanthi V. Synthesis and Characterization of Matryoshka Doll-Like Silica Nanoparticles. In Proceedings of International Conference on Advanced Nanomaterials & Emerging Engineering Technologies, Chennai, India, 24-26 July 2013. https://doi.org/*10.1109/ICANMEET.2013.6609234*
6. Ghosh, S.; Hiser, J. D..; Davidson, J. W. Matryoshka: Strengthening Software Protection via Nested Virtual Machines. In Proceedings of IEEE/ACM International Workshop on Software Protection, Florence, Italy, 19 May 2015. https://doi.org/10.1109/SPRO.2015.11
7. Leroux, S.; Bohez, S.; De Coninck, E.; Verbelen, T.; Vankeirsbilck, B.; Simoens, P.; Dhoedt, B. Multi-Fidelity Matryoshka Neural Networks for Constrained IoT Devices. In Proceedings of International Joint Conference on Neural Networks, Vancouver, BC, Canada, 24-29 July 2016. https://doi.org/10.1109/IJCNN.2016.7727348
8. Kyaw, Z.; Qi, S.; Gao, K.; Zhang, H.; Zhang, L.; Xiao, J.; Wang, X.; Chua, T.-S. Matryoshka Peek: Toward Learning Fine-Grained, Robust, Discriminative Features for Product Search. *IEEE Transactions on Multimedia* **2017**, *19*, 1272-1284. https://doi.org/10.1109/TMM.2017.2655422

9. Richter, S. R.; Roth, S. Matryoshka Networks: Predicting 3D Geometry via Nested Shape Layers. In Proceedings of IEEE/CVF Conference on Computer Vision and Pattern Recognition, Salt Lake City, UT, USA, 18-23 June 2018. https://doi.org/10.1109/CVPR.2018.00207
10. Shinmura, S. Cancer Gene Analysis of Microarray Data. In Proceedings of IEEE/ACIS International Conference on Big Data, Cloud Computing Data Science & Engineering, Yonago, Japan, 12-13 July 2108. https://doi.org/10.1109/BCD2018.2018.00009
11. Malik, L.; Patro. R. Rich Chromatin Structure Prediction from Hi-C Data. *IEEE/ACM Transactions on Computational Biology and Bioinformatics* **2019**, *16*, 1448-1458. https://doi.org/10.1109/TCBB.2018.2851200
12. Sun, M.; Pu, L.; Zhang, J.; Xu, J. Matryoshka: Joint Resource Scheduling for Cost-Efficient MEC in NGFI-Based C-RAN. In Proceedings of IEEE International Conference on Communications, Shanghai, China, 20-24 May 2019. https://doi.org/10.1109/ICC.2019.8762044
13. Pozza, M.; Nicholson, P. K.; Lugones, D. F.; Rao, A.; Flinck, H.; Tarkoma, S. On Reconfiguring 5G Network Slices. *IEEE Journal on Selected Areas in Communications* **2020**, *38*, 1542-1554. https://doi.org/10.1109/JSAC.2020.2986898
14. Zhu, Y.; Zhao, Z.; Du, L. Matryoshka Phononic Crystals for Anchor-Loss Reduction of Lamb Wave Resonators. In Proceedings of IEEE International Conference on Nanotechnology, Montreal, QC, Canada, 29-31 July 2020. https://doi.org/10.1109/NANO47656.2020.9183689
15. Huang, H.; Zhong, J.; Taku, K. Matryoshka Attack: Research on an Attack Method of Recommender System Based on Adversarial Learning and Optimization Solution. In Proceedings of International Conference on Wavelet Analysis and Pattern Recognition, Adelaide, Australia, 2 December 2020. https://doi.org/10.1109/ICWAPR51924.2020.9494616
16. Drimmel, R.; Sozzetti, A.; Schröder, K.-P.; Bastian, U.; Pinamonti, M.; Jack, D.; Huerta, M. A. H. A Celestial Matryoshka: Dynamical and Spectroscopic Analysis of the Albireo System. *Monthly Notices of the Royal Astronomical Society*, **2019**, *502*, 1-17. https://doi.org/10.1093/mnras/staa4038
17. Ferreira, H. P. A. Matryoshka: A Geometry Proposal for Multiband Frequency Selective Surfaces (in Portuguese). MSc Thesis, Instituto Federal da Paraíba, João Pessoa, Brazil, March 2014. https://repositorio.ifpb.edu.br/handle/177683/274
18. Neto, A. G.; D'Assunção Junior, A. G.; Silva, J. C.; Silva, A. N.; Ferreira, H. P. A.; Lima, I. S. S. A Proposed Geometry for Multi-Resonant Frequency Selective Surfaces. In Proceedings of the European Microwave Conference, Rome, Italy, 6-9 October 2014. https://doi.org/10.1109/EuMC.2014.6986580
19. Cruz, J. N. Characterization of a FSS with Open Matryoshka Geometry (in Portuguese). MSc Thesis, Instituto Federal da Paraíba, João Pessoa, Brazil, July 2015. https://repositorio.ifpb.edu.br/handle/177683/240
20. Mariano, J. G. O. Implementation of Planar Filters Based on a Matryoshka Geometry (in Portuguese). MSc Thesis, Instituto Federal da Paraíba, João Pessoa, Brazil, March 2017. https://repositorio.ifpb.edu.br/handle/177683/298
21. Sousa, T. R. Development of Frequency Selective Surfaces Based on a Polarization Independent Matryoshka Geometry (in Portuguese). MSc Thesis, Instituto Federal da Paraíba, João Pessoa, Brazil, January 2019. https://repositorio.ifpb.edu.br/handle/177683/878
22. Neto, J. A. S. Use of Metamaterial Resonators to Improve the Performance of Planar Filters (in Portuguese). MSc Thesis, Federal University of Rio Grande do Norte, Natal, Brazil, December 2019. https://repositorio.ufrn.br/handle/123456789/30834
23. Coutinho, I. B. G. Development of Frequency Selective Surfaces with Combination of Crossed Dipole and Matryoshka Geometries (in Portuguese). MSc Thesis, Instituto Federal da Paraíba, João Pessoa, Brazil, February 2020. https://repositorio.ifpb.edu.br/handle/177683/1319
24. Alencar, M. O. Development of a Bandpass FSS Based on a Matryoshka Geometry (in Portuguese). MSc Thesis, Instituto Federal da Paraíba, João Pessoa, Brazil, April 2020. https://repositorio.ifpb.edu.br/handle/177683/998
25. Santos, M. G. A. R. Research on the Use of Resonators with Matryoshka Geometry in Planar Antennas (in Portuguese). MSc Thesis, Instituto Federal da Paraíba, João Pessoa, Brazil, June 2020. https://repositorio.ifpb.edu.br/handle/177683/1776
26. Neto, A. F. Planar Filters Based on a Matryoshka Geometry with Rectangular and Circular Rings (in Portuguese). MSc Thesis, Instituto Federal da Paraíba, João Pessoa, Brazil, July 2020. https://repositorio.ifpb.edu.br/handle/177683/999
27. Duarte, L. M. S. Reconfigurable Frequency Selective Surfaces Using PIN Diodes and RF Inductors Combining Crossed Dipole and Matryoshka Geometries (in Portuguese). MSc Thesis, Instituto Federal da Paraíba, João Pessoa, Brazil, July 2021. https://repositorio.ifpb.edu.br/handle/177683/1819
28. Souto, A. H. P. Analysis of the Radiation Characteristics of Microstrip Patch Antennas in the 3.5 GHz Frequency Band Using Resonators with Matryoshka Geometry (in Portuguese). MSc Thesis, Instituto Federal da Paraíba, João Pessoa, Brazil, March 2023. https://repositorio.ifpb.edu.br/handle/177683/3135

29. Abreu, F. A. T. Matryoshka Geometry Used in a DGS Sensor (in Portuguese). MSc Thesis, Instituto Federal da Paraíba, João Pessoa, Brazil, May 2023. https://repositorio.ifpb.edu.br/handle/177683/3267
30. Santos, D. A. DGS Filters Based on the Matryoshka Geometry (in Portuguese). MSc Thesis, Instituto Federal da Paraíba, João Pessoa, Brazil, May 2023. https://repositorio.ifpb.edu.br/handle/177683/3266
31. Albuquerque, B. L. C. Development of a Soil Humidity Sensor Using a DGS Based on the Matryoshka Geometry (in Portuguese). MSc Thesis, Instituto Federal da Paraíba, João Pessoa, Brazil, July 2023. https://repositorio.ifpb.edu.br/handle/177683/3259
32. Neto, A. G.; D'Assunção Junior, A. G.; Silva, J. C.; Cruz, J. N.; Silva, J. B. O.; Ramos, N. J. P. L. Multiband Frequency Selective Surface with Open Matryoshka Elements. In Proceedings of European Conference on Antennas and Propagation, Lisbon, Portugal, 12-17 April 2015. https://ieeexplore.ieee.org/stamp/stamp.jsp?tp=&arnumber=7228440
33. Neto, A. G.; Silva, J. C.; Carvalho, J. N.; Cruz, J. N.; Ferreira H. P. A. Analysis of the Resonant Behavior of FSS Using Matryoshka Geometry. In Proceedings of IEEE/SBMO MTT-S International Microwave and Optoelectronics Conference, Porto de Galinhas, PE, Brazil, 3-6 November 2015. https://doi.org/10.1109/IMOC.2015.7369142
34. Neto, A. G.; Costa Junior, A. G.; Moreira, C. S.; Sousa, T. R.; Coutinho, I. B. G. A New Planar Sensor Based on the Matryoshka Microstrip Resonator. In Proceedings of IEEE/SBMO MTT-S International Microwave and Optoelectronics Conference, Águas de Lindoia, SP, Brazil, 27-30 August 2017. https://doi.org/10.1109/IMOC.2017.8121074
35. Ferreira, H. P. A.; Serres A. J. R.; Assis, F. M.; Carvalho J. N. A Multi-Resonant Circuit Based on Dual-Band Matryoshka Resonator for Chipless RFID Tag. In Proceedings of European Conference on Antennas and Propagation, London, UK, 9-13 April 2018. https://doi.org/10.1049/cp.2018.1169
36. Neto, A. G.; Sousa, T. R.; Silva, J. C.; Mamedes, D. F. A Polarization Independent Frequency Selective Surface Based on the Matryoshka Geometry. In Proceedings of IEEE/MTT-S International Microwave Symposium, Philadelphia, PA, USA, 10-15 June 2018. https://doi.org/10.1109/MWSYM.2018.8439231
37. Neto, A. G.; Neto, A. F.; Andrade, M. C.; Silva, J. C.; Carvalho, J. N. Stop-Band Compact Filter with Reduced Transition Region for Application in the 2.4 GHz Frequency Band (In Portuguese). In Proceedings of the Brazilian Symposium of Telecommunications and Signal Processing, Campina Grande, PB, Brazil, 16-19 September 2018. https://biblioteca.sbrt.org.br/articles/1708
38. Neto, A. G.; Silva, J. C.; Coutinho, I. B. G.; Alencar, M. O.; Albuquerque, I. F.; Santos, B. L. G. Polarization Independent Triple-Band Frequency Selective Surface Based on Matryoshka Geometry. In Proceedings of IEEE/SBMO MTT-S International Microwave and Optoelectronics Conference, Aveiro, Portugal, 10-14 November 2019. https://doi.org/10.1109/IMOC43827.2019.9317588
39. Neto, A. G.; Silva, J. C.; Serres, A. J. R.; Alencar, M. O.; Coutinho, I. B. G.; Evangelista, T. S. Dual-Band Pass-Band Frequency Selective Surface Based on the Matryoshka Geometry with Angular Stability and Polarization Independence. In Proceedings of European Conference on Antennas and Propagation, Copenhagen, Denmark, 15-20 March 2020. https://doi.org/10.23919/EuCAP48036.2020.9135542
40. Neto, A. G.; Silva, J. C.; Coutinho, I. B. G.; Alencar, M. O.; Andrade, D. M. Triple Stop-Band Frequency Selective Surface with Application to 2.4 GHz Band. *Journal of Communication and Information System* **2020**, *35*, 77-85. https://doi.org/
41. Mamedes, D. F.; Neto, A. G.; Bornemann, J.; Silva, J. C.; Abreu, F. A. T. A Sensor Using a Matryoshka Geometry Defected Ground Structure. In Proceedings of European Conference on Antennas and Propagation, Madrid, Spain, 27 March-1 April 2022. https://doi.org/10.23919/EuCAP53622.2022.9768950
42. Bhope, V.; Harish, A. R. Polarization Insensitive Miniaturized Multiband FSS using Matryoshka Elements. In Proceedings of IEEE International Symposium on Antennas and Propagation and USNC-URSI Radio Science Meeting, Denver, CO, USA, 10-15 July 2022. https://doi.org/10.1109/AP-S/USNC-URSI47032.2022.9887292
43. Neto, A. G.; Carvalho, J. N.; Silva, J. C.; Lima, C. G. M.; Raimundo, R. A.; Macedo, D. A. Miniaturization of DGS Filter Based on Matryoshka Geometry Using Calcium Cobaltite Ceramic. In Proceedings of IEEE/SBMO MTT-S International Microwave and Optoelectronics Conference, Castelldefels, Barcelona, Spain, 5-9 November 2023.
44. Albuquerque, B. L. C.; Nóbrega, G. K.; Ferreira, M. S.; D'Andrea A.; Carvalho, J. N.; Neto, A. G. A New Soil Moisture Sensor Based on Matryoshka DGS. In Proceedings of IEEE/SBMO MTT-S International Microwave and Optoelectronics Conference, Castelldefels, Barcelona, Spain, 5-9 November 2023.
45. Silva, J. C.; Neto, A. G.; Abreu, F. A. T.; Santos, D. A.; Peixeiro, C.; Lopes, M. E. S. Comparison of Two Sensors with Matryoshka Defected Ground Structures. In Proceedings of IEEE/SBMO MTT-S International Microwave and Optoelectronics Conference, Castelldefels, Barcelona, Spain, 5-9 November 2023.
46. Neto, A. G.; Costa, J. A.; Cavalcante, G. A.; Henrique, R. L.; Santos, L. K. L. Numerical Results for a Pass-Band Filter Based on a Matryoshka Geometry Using Three Metal Layers (in Portuguese). In Proceedings of the Symposium on Research, Innovation and Postgraduation at Federal Institute of Paraiba, João Pessoa, PB, Brazil, 22-24 November 2023.

47. Baena, J. D.; Bonache, J.; Martín, F.; Sillero, R. M.; Falcone, F.; Lopetegi, T.; Laso, M. A. G.; García-García, J.; Gil, I.; Portillo, M. F.; Sorolla, M. Equivalent-Circuit Models for Split-Ring Resonators and Complementary Split-Ring Resonators Coupled to Planar Transmission Lines. *IEEE Transactions on Microwave Theory and Techniques* **2005**, 53, 1451-1461. https://doi.org/10.1109/TMTT.2005.845211
48. Kim, C.-S.; Park, J.-S.; Ahn, D.; Lim, J.-B. A Novel 1-D Periodic Defected Ground Structure for Planar Circuits. *IEEE Microwave and Guided Wave Letters* **2000**, 10, 131-133. https://doi.org/10.1109/75.846922
49. Hong, J.-S.; Lancaster, M. J. *Microstrip Filters for RF/Microwave Applications*, John Wiley & Sons: New York, USA, 2001.
50. https://www.ansys.com/products/electronics/ansys-hfss
51. Munk, B. A. *Frequency Selective Surfaces: Theory and Design*, John Wiley & Sons: New York, USA, 2000.
52. Vardaxoglou, J. C. *Frequency Selective Surfaces: Analysis and Design*, Research Studies Press: Taunton, England, 1997.
53. Bohra, H.; Prajapati, G. Microstrip filters: a review of different filter designs used in ultrawide band technology. *Makara Journal of Technology* **2020**, 24, 79-86. https://doi.org/10.7454/mst.v24i2.3903
54. Fu, W.; Li, Z.-M.; Cheng, J.-W.; Qiu, X. A Review of Microwave Filter Designs Based on CMRC. In Proceedings of the IEEE MTT-S International Wireless Symposium (IWS), Shanghai, China, 20-23 September 2020. https://doi.org/10.1109/IWS49314.2020.9360131
55. Edwards, T. C.; Steer, M. B. *Foundations of Interconnected and Microstrip Design*, 3rd Edition; John Wiley& Sons: Chichester, UK, 2000.
56. Neto, A. G.; Carvalho, J. N.; Mariano, J. G. O.; Sousa, T. R. Analysis of the application of matryoshka geometry to microstrip filters. (In Portuguese). In Proceedings of the Brazilian Congress of Electromagnetism and Brazilian Symposium on Microwaves and Optoelectronics (MOMAG), Porto Alegre, RS, Brazil, 25-29 July 2016.
57. Pandit, S.; Ray, P.; Mohan, A. Compact MIMO antenna enabled by DGS for WLAN applications. Proceedings of IEEE International Symposium on Antennas and Propagation & USNC/URSI National Radio Science Meeting, Boston, MA, USA, 8-13 July 2018. https://doi.org/10.1109/APUSNCURSINRSM.2018.8609389
58. Souza, F. A. A.; Campos, A. L. P. S.; Neto, A. G.; Serres, A. J. R.; Albuquerque, C. C. R. Higher Order Mode Attenuation in Microstrip Patch Antenna with DGS H Filter Specification from 5 to 10 GHz Range. Journal of Microwaves, Optoelectronics and Electromagnetic Applications **2020**, 19, 214–227. https://doi.org/10.1590/2179-10742020v19i2823
59. J. Zhou, J.; Rao, Y.; Yang, D.; Qian, H. J.; Luo, X. Compact wideband BPF with wide stopband using substrate integrated defected ground structure. *IEEE Microwave and Wireless Components Letters* 2021, 31, 353-356. https://doi.org/10.1109/LMWC.2021.3053756
60. Cao, S.; Han, Y.; Chen, H.; Li J. An Ultra-Wide Stop-Band LPF Using Asymmetric Pi-Shaped Koch Fractal DGS. *IEEE Access* **2017**, 5, 27126-27131. https://doi.org/10.1109/ACCESS.2017.2773577
61. Farooq, M.; Abdullah, A.; Zakir, M. A.; Cheema H. M. Miniaturization of a 3-way power divider using defected ground structures. Proceedings of IEEE Asia-Pacific Microwave Conference (APMC), Singapore, 10-13 December 2019. https://doi.org/10.1109/APMC46564.2019.9038858
62. Oh S.; , Koo, J.-J.; Hwang, M.S.; Park, C.; Jeong, Y.-C.; Lim, J.-S.; Choi, K.-S.; Ahn, D. An unequal Wilkinson power divider with variable dividing ratio. Proceedings of IEEE/MTT-S International Microwave Symposium, Honolulu, HI, USA, 3-8 June 2007. https://doi.org/10.1109/MWSYM.2007.380475
63. Mansour, E.; Allam, A.; Abdel-Rahman A. B. A novel approach to non-invasive blood glucose sensing based on a defected ground structure. Proceedings of European Conference on Antennas and Propagation (EuCAP), Dusseldorf, Germany, 22-26 March 2021. https://doi.org/10.23919/EuCAP51087.2021.9411425
64. Oliveira, J. G. D.; Duarte Junior, J. G.; Pinto, E. N. M. G.; Neto, V. P. S.; D'Assunção, A. G. A new planar microwave sensor for building materials complex permittivity characterization. *Sensors* 2020, 20, 6328. https://doi.org/**10.3390/s20216328**
65. Dautov, K.; Hashmi, M.; Nauryzbayev, G.; Nasimuddin, N. Recent advancements in defected ground structure-based near-field wireless power transfer systems. *IEEE Access* **2020**, 8, 81298-81309. https://doi.org/10.1109/ACCESS.2020.2991269
66. Hekal, S.; Abdel-Rahman, A. B.; Jia, H.; Allam, A.; Barakat, A.; Pokharel, R. K. A novel technique for compact size wireless power transfer applications using defected ground structures. *IEEE Transactions on Microwave Theory and Techniques*, **2017**, 65, 591-599. https://doi.org/10.1109/TMTT.2016.2618919
67. Neto, A. G.; Silva, J. C.; Coutinho, I. B. G.; Camilo Filho, S. S.; Santos, D. A.; Albuquerque, B. L. C. A Defected Ground Structure Based on Matryoshka Geometry. *Journal of Microwaves, Optoelectronics and Electromagnetic Applications* **2022**, 21 284–293. https://doi.org/10.1590/2179-10742022v21i2256115
68. Peixeiro, C. Microstrip Antenna Papers in the IEEE Transactions on Antennas and Propagation. *IEEE Antennas and Propagation Magazine* **2012**, 54, 264-268. https://doi.org/10.1109/MAP.2012.6202561
69. Arya, A. K.; Kartikeyan, M. V.; Patnaik, A. Defected Ground Structure in the Perspective of Microstrip Antennas: A Review. *Frequenz* **2010**, 64, 79-84. https://doi.org/10.1515/FREQ.2010.64.5-6.79

70. Khandelwal, M. K; Kanaujia, B. K.; Kumar, S. Defected Ground Structures: Fundamentals, Analysis, and Applications in Modern Wireless Trends. *International Journal of Antennas and Propagation* **2017**, 1-22. https://doi.org/10.1155/2017/2018527
71. Sung, Y. J.; Kim, S.; Kim, Y.-S. Harmonics Reduction with Defected Ground Structure for a Microstrip Patch Antenna. *IEEE Antennas and Wireless Propagation Letters* **2003**, 2, 111-113. https://doi.org/10.1109/LAWP.2003.815281
72. Mishra, B.; Singh, V.; Singh, R. K.; Singh, N.; Singh, R. A Compact UWB Patch Antenna with Defected Ground for Ku/K Band Applications. Microwave Optical and Technology Letters **2017**, 60, 1-6. https://doi.org/**10.1002/mop.30911**
73. Guha, D.; Biswas, M.; Antar, Y. M. M. Microstrip Patch Antenna with Defected Ground Structure for Cross Polarization Supression. *IEEE Antennas and Wireless Propagation Letters* **2005**, 4, 455-458. https://doi.org/10.1109/LAWP.2005.860211
74. Dwivedy, B. Consideration of Engineered Ground Planes for Planar Antennas: Their Effects and Applications, a Review. *IEEE Access* **2022**, 10, 84317-84329. https://doi.org/10.1109/ACCESS.2022.3195507
75. Pendry, J. B.; Holden, A. J.; Robbins, D. J.; Stewart, W. J. Magnetism from Conductors and Enhanced Nonlinear Phenomena. *IEEE Transactions on Microwave Theory and Techniques* **1999**, 47, 2075-2084. https://doi.org/10.1109/22.798002
76. Balanis, C. A. Antenna Theory: Analysis and Design. 4th ed.; John Wiley & Sons: New York, USA, 2015; pp. 788-814.
77. https://www.ansys.com/
78. Fraden, J. *Handbook of Modern Sensors: Physics, Designs, and Applications*, 4th ed.; Springer: New York, USA, 2010.
79. Patricio, M. C. Z. B.; Santos, P. S.; Silva, J. C.; Carvalho, J. N.; Neto, A. G. Determination of Sucrose Dilution Level in Aqueous Solution Using a DGS Sensor Based on Matryoshka Geometry (In Portuguese). In Proceedings of the Brazilian Symposium of Microwaves and Optoelectronics (SBMO), Natal, RN, Brazil, 13-16 November 2022.